[AMERICAN JOURNAL OF SCIENCE, VOL. 289, JUNE, 1989, P. 661–707]

American Journal of Science

JUNE 1989

SULFUR ISOTOPIC VARIATIONS AMONG MINERALS AND AQUEOUS SPECIES IN THE SALTON SEA GEOTHERMAL SYSTEM: A SHRIMP ION MICROPROBE AND CONVENTIONAL STUDY OF ACTIVE ORE GENESIS IN A SEDIMENT-HOSTED ENVIRONMENT

MICHAEL A. MCKIBBEN* and C. STEWART ELDRIDGE**

ABSTRACT. In situ SHRIMP ion microprobe and conventional techniques were used to determine the sulfur isotopic compositions of accessible sulfur-bearing phases in the Salton Sea geothermal system including: diagenetic sulfate and sulfide minerals in the lacustrine-deltaic host sediments, sulfide minerals in intrusive igneous rocks, sulfate and sulfide minerals in hydrothermal veins, and aqueous SO_4 and H_2S in hydrothermal fluids. Microscopic sulfur isotopic heterogeneity within sulfide and sulfate minerals, found using SHRIMP, spans a range that is more than twenty times the 2 permil analytical uncertainty, highlighting the advantages afforded by the 30 μm spatial resolution of the ion probe.

Diagenetic sulfate and sulfide minerals in the host sediments formed in an upward regressional continental sabkha environment. The apparent fractionation between intergrown diagenetic anhydrite and pyrite is typically near 20 permil but ranges from 7 to 40 permil. There is no approach toward equilibrium isotopic partitioning with increased burial and heating of the sediments to greenschist and lower amphibolite facies metamorphic conditions, suggesting that these minerals have retained their original diagenetic isotopic compositions. $\delta^{34}S$ variations in anhydrite are as great as 13 permil in the space of only 0.25 mm, indicating the importance of closed-system fractionation effects during diagenetic growth. Sedimentary pyrite exhibits sequential overgrowths recording large shifts in $\delta^{34}S$ from as low as -48 permil to as high as -9 permil in the space of only 0.25 mm, likely formed during the transition from open to closed-system bacterial sulfate reduction accompanying sediment burial diagenesis.

Hydrothermal vein sulfide minerals show a bimodal $\delta^{34}S$ distribution, with most clustering near 0 permil (-9 to 9 permil). $\delta^{34}S$ variations of as much as 10 permil occur in a space of only 1 mm in a chalcopyrite vein, possibly reflecting closed-system fractionation

* Department of Earth Sciences and Geothermal Resources Program of the Institute of Geophysics and Planetary Physics, University of California, Riverside, California, 92521.

** Geology Department and Research School of Earth Sciences, The Australian National University, G.P.O. Box 4, Canberra, A.C.T. 2601, Australia

effects during precipitation. A second group of older, isotopically light veins (−25 to −20 permil) in a thick shale probably contains H_2S derived from catagenesis of local organic matter. Samples containing intergrown vein and sedimentary sulfides show no evidence of recycling of pre-existing biogenic sulfide into the hydrothermal mineralization and no evidence of hydrothermal overgrowths on sedimentary pyrite. Differences as great as 30 permil are preserved between diagenetic pyrite and enveloping vein chalcopyrite, indicating that the metal-rich, sulfur-poor hydrothermal brines simply do not react with sedimentary pyrite in the host rocks. The textures and isotopic compositions of sulfides associated with a thin 3 km deep diabase sill (−7 to −1 permil) suggest that it has been veined and hydrothermally altered but was not a major source of sulfur for vein mineralization. Younger magma responsible for rhyolite domes at the surface could be a source of ≈0 permil sulfur, but no silicic intrusions have yet been penetrated by drilling, and the surface domes contain no obvious primary sulfide.

H_2S and SO_4 in deep hypersaline brines are in isotopic equilibrium (Δ = 18–19 permil at 300°–320°C), demonstrating that high salinity (25 wt percent TDS) does not affect equilibrium isotope partitioning. The mean $\delta^{34}S$ of brine H_2S (≈0 permil) coincides with that of the main group of vein sulfides, but brine SO_4 ($\delta^{34}S$ ≈20 permil) is consistently enriched in ^{34}S by ≈10 permil relative to host rock anhydrite (mean $\delta^{34}S$ ≈10 permil). The directly-measured isotopic composition of total sulfur in the brines (≈10 permil) is consistent with derivation of the H_2S by hydrothermal reduction of SO_4 derived from metaevaporitic anhydrite in the host sediments. Partial replacement of anhydrite by epidote and tremolite observed at depth also supports this scenario. Secondary contributions of sulfur from dissolution of biogenic sulfide contained in the sedimentary anhydrite, local catagenesis of organic matter in shales, and degassing or leaching of igneous intrusions could account for some of the variations in $\delta^{34}S$ of vein sulfides.

INTRODUCTION

Much of our understanding of sulfur isotope systematics in hydrothermal systems comes from studies of fossil geothermal systems now mined as ore deposits (Ohmoto, 1986; Ohmoto and Rye, 1979; Rye and Ohmoto, 1974; Taylor, 1987). Such studies are important because of the extent of the exposures and the great volume of mineralized material available for sampling, among other features. However, the investigation of inter- and intramineral isotopic variations in ore deposits has provided only indirect evidence of the sulfur speciation and isotopic composition of ore-forming fluids. Moreover, the task of distinguishing those features formed during the original ore depositional events and those overprinted during subsequent metamorphism and tectonism has not always been easy.

Studies of active geothermal systems are less prone to the complications of metamorphic overprinting and provide opportunities to sample directly cogenetic solids and fluids as well as to measure temperatures

and pressures. Additionally, the element source areas and transport pathways feeding active systems can often be deduced and sampled; in fossil systems such regional features may be removed or obliterated by later tectonic processes.

Recently, several sulfur isotopic studies have been focused on recently-discovered active oceanic hydrothermal systems (Shanks and Seyfried, 1987, and references cited therein). In particular Shanks and Seyfried (1987) report the first $\delta^{34}S$ study of cogenetic sulfides and fluids from active seafloor vent deposits, concluding that sulfur for ore formation is derived from igneous H_2S which mixes with H_2S derived from reduction of seawater sulfate in the vents. While these studies represent an advance over traditional ore deposit investigations, the technical difficulties of deep drilling in mid-ocean ridge environments have limited such investigations to the uppermost portions of submarine hydrothermal systems.

Although continental geothermal systems offer much easier drilling conditions, few systems have been found that transport and deposit appreciable amounts of metals and sulfur. The few sulfur isotopic studies of continental systems have been mainly of a reconnaissance nature and have emphasized low-salinity volcanic-hosted systems (Arnold and Partida, 1987; Browne, Rafter, and Robinson, 1975; Kusakabe, 1974; Schoen and Rye, 1970; Steiner and Rafter, 1966; Torssander, 1986; Truesdell and others, 1978). No study has examined comprehensively the sulfur isotopic geochemistry of host rocks, mineralization, and fluid species within a saline system.

The present study involves a systematic investigation of the sulfur isotopic variations in sulfide and sulfate minerals of the host sediments, sulfides in igneous rocks, vein sulfide minerals, and oxidized and reduced sulfur species in hydrothermal fluids from the Salton Sea geothermal system. The samples for our study were provided by the Salton Sea Scientific Drilling Project (Elders and Sass, 1988), the first deep continental scientific drilling project in the United States. Our data have been used to elucidate: (1) biogenic SO_4-H_2S fractionation during host rock sedimentation in a saline lake environment, (2) the extent of isotopic re-equilibration of diagenetic sulfide and sulfate during prograde hydrothermal metamorphism of the host sediments, (3) the degree of isotopic equilibration between H_2S and SO_4 in hypersaline geothermal brines, (4) the role of hydrothermal sulfate reduction in generating reduced sulfur for ore genesis, (5) the contributions of different potential sulfur sources to vein sulfide mineralization, and (6) how far mineral textural data alone should be extrapolated in defining the history of ore-forming events.

SALTON SEA GEOTHERMAL SYSTEM

The Salton Sea geothermal system (SSGS) is located in the Salton Trough of southern California (fig. 1), an active continental rift-zone forming the landward extension of the Gulf of California-East Pacific

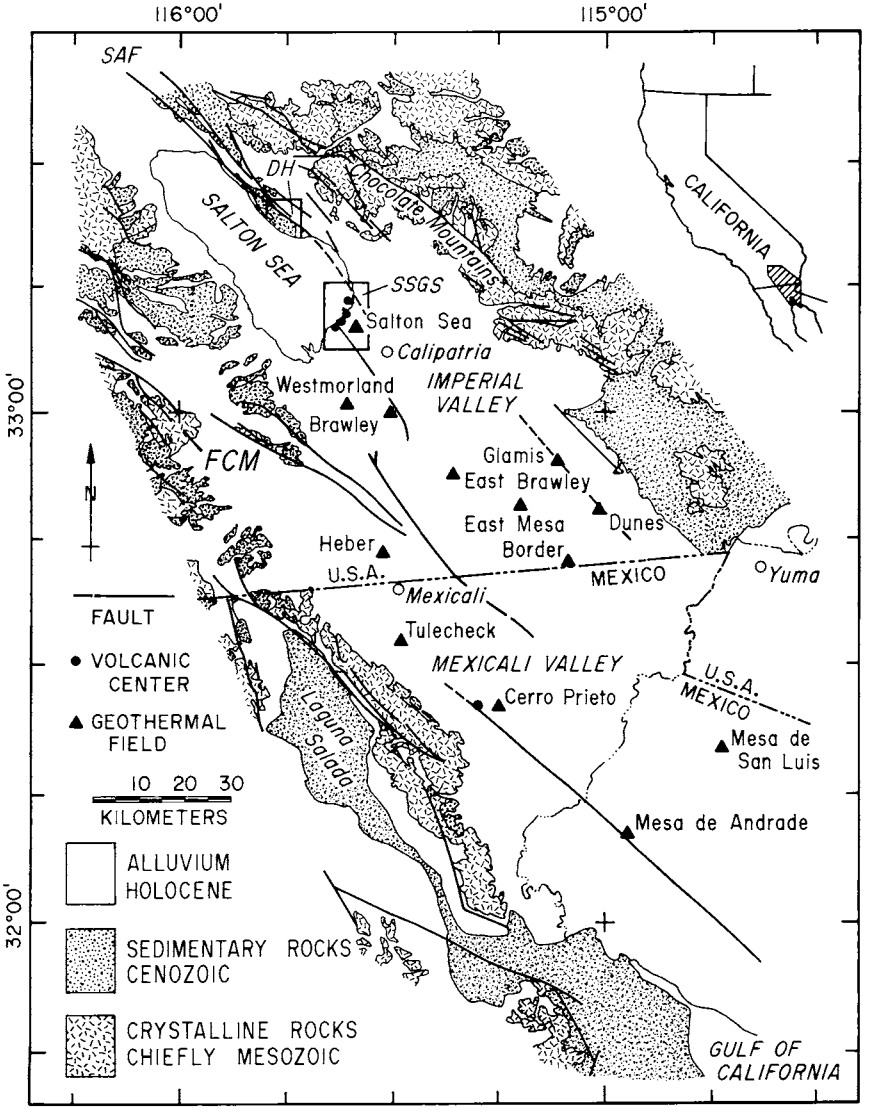

Fig. 1. Map of the Salton Trough of southern California and northern Baja California, showing the locations of active geothermal fields and Quaternary volcanic centers. The Colorado River enters the rift near Yuma and presently meanders south to the Gulf of California. SSGF = Salton Sea geothermal field. DH = Durmid Hills. FCM = Fish Creek Mountains.

Rise oceanic spreading system (Elders and others, 1972). The delta of the Colorado River, which enters the Trough from the east, has filled the rift as it has opened, isolating the closed, evaporative Salton Sea basin from the Gulf of California for the last 4 Ma (Elders, 1979; Winker and Kidwell, 1986).

CO_2 mudpots and an arc of five Quaternary rhyolite domes (fig. 2) are the only obvious surface expressions of the SSGS thermal anomaly (Helgeson, 1968; Muffler and White, 1969; Robinson, Elders, and Muffler, 1976). At drilled depths of 2 to 4 km, Pleistocene fluvial and lacustrine deltaic deposits derived from the Colorado River are progressively metamorphosed to hornfels containing low-pressure greenschist and amphibolite facies mineral assemblages (Muffler and White, 1969; McDowell and Elders, 1980, 1983; Cho, Liou, and Bird, 1988). Because the area exhibits evidence of geologically young surface rhyolitic volcanic activity (Robinson, Elders, and Muffler, 1976) and diabase sills have been encountered at depth during drilling (Browne and Elders, 1976; Elders, 1987; Herzig and Elders, 1988), it is logical to infer a magmatic heat source for the thermal anomaly.

Several early studies focused on the hypersaline brines and resultant metal-rich pipe-scales (White, Anderson, and Grubbs, 1963; Skinner and others, 1967; White, 1968; Helgeson, 1968). The brines are very deficient in sulfur relative to metals, so that the availability of reduced sulfur remains the major limitation on ore-formation (Skinner and others, 1967). A few $\delta^{34}S$ values (-1.4 to 3 permil) for vein sulfides and pipe scales tentatively implied a magmatic origin for the reduced sulfur (White, 1968).

The first detailed investigation of ore mineralization was reported by McKibben and Elders (1985). Their study of drill cuttings revealed that two sets of ore-bearing veins were present in the SSGS: (type 1) an older, more reduced, and possibly more sulfur-rich assemblage, and (type 2) a younger assemblage precipitating from the more oxidized, sulfur-poor modern brines. Both phase equilibria and fluid chemical analyses indicated that the modern hypersaline brines contained subequal amounts of H_2S and SO_4, with an f_{O_2} near the pyrite-hematite boundary at $\simeq$300°C. McKibben and Elders (1985) also noted the occurrence of stratiform diagenetic sulfides in the deltaic sediments and observed textures suggesting that hydrothermal sulfides sometimes enveloped diagenetic stratiform pyrite, concluding that sedimentary iron sulfides may be an additional source of sulfur for ore mineralization.

Recently, studies of new drillcores recovered by the Salton Sea Scientific Drilling Project (SSSDP) and by commercial drilling have dramatically clarified many aspects of ore mineralization in the SSGS. Additionally, ongoing commercial development of the geothermal field has provided opportunities to sample fluids from multiple depths. Distinct sources of water, salinity, and dissolved metals are now recognized, and a model has been proposed for the formation of the modern

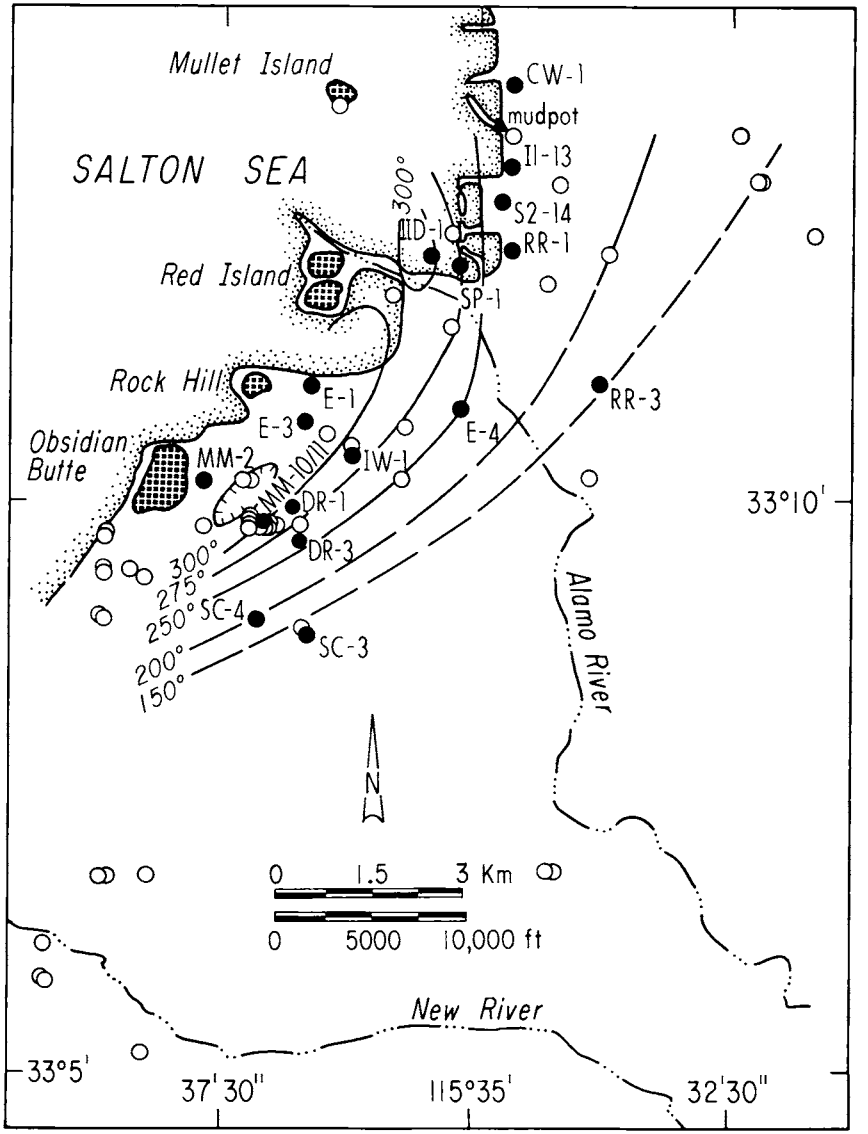

Fig. 2. Map of the Salton Sea geothermal field, showing the locations of geothermal wells (circles). Filled circles denote the wells used in this study. Arc of five Quaternary volcanic domes is indicated by grid pattern; shoreline of modern Salton Sea is indicated by stippled pattern. Contours are isotherms of subsurface temperatures (°C) at depth of 914 m (3000 ft).

(type 2) vein ore minerals by mixing at a sharp interface between a hot upwelling hypersaline brine diapir and overlying lower salinity fluids (McKibben and others, 1987; McKibben, Williams, and Okubo, 1988; McKibben, Andes, and Williams, 1988; Williams, 1988; Williams and McKibben, 1989).

The new cores also revealed that significant amounts of metamorphosed lacustrine evaporites, rich in $CaSO_4$, are present in the SSGS host rocks at 1 to 3 km depth (Herzig, Mehegan, and Stelting, 1988; McKibben, Williams, and Okubo, 1988; Osborn, ms; Osborn, McKibben, and Williams, 1988). This occurrence adds another possible mechanism of generating reduced sulfur: hydrothermal reduction of evaporite-derived SO_4. Also, a sulfide-bearing diabase sill and its lower contact zone were cored at 3 km depth in the SSSDP borehole (Elders, 1987; Herzig and Elders, 1988). This discovery resurrects White's (1968) model for injection of juvenile magmatic sulfur into the geothermal system. The new cores and fluids thus provided the samples necessary for testing the relative importance of different sources of sulfur for ore mineralization in the SSGS.

High spatial-resolution (30 μm) sulfur isotope analyses of minerals, developed on the SHRIMP ion microprobe in the Research School of Earth Sciences at the Australian National University (Eldridge and others, 1987; Eldridge, 1988b), allows detailed in situ analysis of $\delta^{34}S$ variations among the finely-intergrown minerals characteristically found in sediment-hosted ore mineralization (Eldridge and others, 1985, 1987, 1988a, b, c).

SAMPLE LOCATIONS, SAMPLING TECHNIQUES, AND ANALYTICAL METHODS

Solid Samples

SSGS core and drill cutting samples used in our study contained representative occurrences of: (1) stratiform evaporitic gypsum and anhydrite, (2) stratiform and disseminated pyrite in sediments, (3) pyrite in igneous rocks, and (4) vein sulfides and anhydrite. Total sulfur in the cores ranges from <0.03 to 4.11 wt percent (Shearer and others, 1988); values above $\simeq$1 percent are unusual, reflecting the presence of vein sulfides or concentrations of diagenetic pyrite and anhydrite. Because of their potential as sources of hydrothermal aqueous sulfate, additional material was collected from sulfate outcrops and mines within the Salton Sea basin. Well locations and outcrops are shown in figures 1 and 2.

Core samples came mostly from the 3.2 km deep SSSDP well S2-14 (Elders and Sass, 1988; Herzig, Mehegan, and Stelting, 1988; McKibben, Andes, and Williams, 1988). Additional cores came from the 1 km deep commercial well MM-11 (McKibben, Williams, and Okubo, 1988). Drill cutting samples came from several deep commercial geothermal wells described by McKibben and Elders (1985), McDowell and Elders (1980), and Williams and McKibben (1989), as well as shallow (<100 m)

wells drilled for thermal gradient measurements (Newmark and others, 1986; Newmark, Kasameyer, and Younker, 1988; Yi, 1987).

Material selected for conventional sulfur isotopic analyses totaled 46 samples (table 1): 10 gypsum samples from 4 shallow thermal gradient wells, 9 gypsum samples from 4 deep geothermal wells, 9 sedimentary pyrite samples from 3 deep geothermal wells, 7 vein sulfide samples from 2 deep geothermal wells, 3 vein anhydrite samples from 1 deep geothermal well, and 4 samples from surface sulfate outcrops in the Salton Trough. The samples were analyzed in the Denver U. S. Geological Survey isotope geochemistry laboratories, under the supervision of R. O. Rye, using standard techniques (Ohmoto and Rye, 1979). Table 1 also incorporates conventional isotope analyses from earlier reconnaissance studies of sulfides and sulfates from drillcore (White, 1968, and written commun., 1986).

A total of 219 SHRIMP analyses were completed on polished samples from wells State 2-14 (S2-14), Magmamax-11 (MM-11), and River Ranch 1 (RR-1) (table 2), comprising 41 analyses of stratiform anhydrite, 64 analyses of stratiform and disseminated pyrite, 22 analyses of pyrite associated with igneous rocks, and 92 analyses of vein sulfides. SHRIMP analytical parameters, fractionation corrections, and error calculations were the same as those in Eldridge and others (1987, 1988b). Analyses incorporated use of standards pyrite 2, chalcopyrite 2, pyrrhotite 2, and galena 2 of Eldridge and others (1987), and an anhydrite crystal from the Ajo deposit (Gilluly, 1946) with a conventionally determined $\delta^{34}S$ value of 6.3 permil (C. W. Field and R. A. Both, written commun., 1986). The standard used for sphalerite analyses was from a Japanese kuroko deposit (Eldridge, Barton, and Ohmoto, 1983) with a conventionally determined $\delta^{34}S$ value of 4.3 permil.

Fluid Samples

Samples of aqueous H_2S and SO_4 were collected from flow tests of 12 geothermal wells in the eastern and northeastern SSGS (fig. 2) from 1985 to 1988 (table 3). All but three of these wells produced hypersaline brine; the others produced low salinity or mixed fluid. These two types of SSGS fluids are recognizable by their differing salinities and chemistries and appear to be density-stratified (McKibben and others, 1987; McKibben, Andes, and Williams, 1988; Williams, 1988; Williams and McKibben, 1989). The deep hypersaline brines have measurable amounts of both H_2S (10–30 ppm) and SO_4 (20–120 ppm), but the shallow low salinity geothermal fluids generally do not contain measurable amounts of H_2S and often have high SO_4 contents (500–2000 ppm). It is not known if $S_2O_3^{2-}$ or other intermediate valence sulfur oxyanions are present. The subhorizontal interface between the two fluid types generally coincides with the domal shape of the 250°C isotherm in the SSGS (Williams, 1988; Williams and McKibben, 1989), which varies in depth from 606 to 1515 m (2000–5000 ft) across the geothermal field (fig. 2). Typical chemical compositions of the shallow low salinity fluids

TABLE 1

Conventional $\delta^{34}S$ analyses of solid samples

Well	Sample	Depth m	Depth ft	$\delta^{34}S$
Geothermal well cuttings and core:				
IID 1[1]	pyrite	1021	(3350)	−1.4
	pyrite	1499	(4917)	2.5
	pyrite	1500	(4923)	3.0
SP-1[1]	pyrite	1421	(4662)	−0.3
S2-14	vein pyrrhotite	2479	(8134.5)	−20.4
	vein pyrrhotite	2479	(8134.5)	−20.9
	vein pyrrhotite	2560	(8398)	6.4
SC-4	gypsum in sediments	148	(487)	19.8
		216	(709)	15.4
		246	(808)	12.2
		406	(1331)	12.1
		579	(1901)	11.4
F-3	gypsum in sediments	206	(675)	11.3
		206	(675)	16.0
F-1	pyrite in sediments	1539	(5050)	2.0
		1928	(6325)	1.0
		2169	(7117)	1.6
MM-2	pyrite in sediments	1101	(3615)	−9.5
		1318	(4325)	4.6
	vein anhydrite	1101	(3615)	9.6
		1138	(3735)	9.5
		1166	(3825)	9.7
RR-1	pyrite in sediments	1308	(4290)	−3.3
		1314	(4310)	−3.1
		1405	(4610)	−3.0
		1429	(4690)	−3.1
	vein sphalerite	899	(2948)	−0.6
		908	(2978)	0.8
	vein chalcopyrite	941	(3088)	1.6
		1112	(3650)	0.1
		1119	(3670)	0.4
	gypsum in sediments	259	(850)	7.1
		280	(950)	5.1
Shallow thermal gradient well cuttings:				
6E	gypsum in sediments	6	(20)	−0.7
6E		20	(65)	13.8
6E		20	(65)	13.9
6E		64	(210)	11.6
6N		9	(30)	−19.7
6N		73	(240)	−0.3
7M		38	(125)	8.8
7U		20	(65)	7.8
7U		47	(155)	7.6
7U		53	(175)	8.5
Durmid Hills				
	gypsum bed in surface outcrop			11.6
	thenardite pod at Bertram Mine			0.7
U.S. Gypsum Mine, Fish Creek Mountains:				
	massive gypsum in upper bench			21.1
	massive anhydrite in lower bench			21.1

[1]From White (1968) and written communication (1986).

TABLE 2

Ion microprobe determinations of sulfur isotopic compositions of minerals from Salton Sea geothermal wells

STATE 2-14

Depth (meters)	Depth (feet)	Crater No.	Mineral	Comments	$^{34}S/^{32}S$ Sample	std. error (1σ)	$^{34}S/^{32}S$ Standard	std. error (1σ)	$\delta^{34}S$ Sample	error (2σ)	Δ_{ANH-PY} (permil)
606.1	1987.0	#1	PY	Type 1 vein in sediment	0.042443	0.000034	0.042983	0.000019	-1	2	
"	"	#2	"	"	0.042365	0.000033	"	"	-3	2	
"	"	#3	"	"	0.042554	0.000034	"	"	2	2	
"	"	#4	"	"	0.042408	0.000033	"	"	-2	2	
606.6	1988.7	#1	GN	Type 1 vein in sediment	0.043355	0.000055	0.043815	0.000037	-9	3	
"	"	#2	CCP	"	0.042894	0.000033	0.043414	0.000016	-5	2	
"	"	#3	"	"	0.042822	0.000029	"	"	-7	2	
"	"	#4	"	"	0.042797	0.000029	"	"	-7	2	
"	"	#5	"	"	0.042859	0.000030	"	"	-6	2	
"	"	#6	PY	"	0.042733	0.000030	0.043374	0.000020	-3	2	
"	"	#7	"	"	0.042607	0.000031	"	"	-6	2	
914.3	2997.8	#1	PY	coarse cubes in vein;	0.042597	0.000025	0.043196	0.000014	-2	2	
"	"	#2	"	some rounded corners	0.042632	0.000025	"	"	-1	2	
"	"	#3	"	in chalcopyrite	0.042713	0.000025	"	"	1	2	
"	"	#4	"	"	0.042649	0.000025	"	"	-1	2	
"	"	#5	CCP	Type 2 vein; with pyrite	0.042732	0.000027	0.043173	0.000020	-3	2	
"	"	#6	"	"	0.042978	0.000028	"	"	2	2	
"	"	#7	"	"	0.043007	0.000028	"	"	3	2	
"	"	#8	"	"	0.042935	0.000028	"	"	1	2	
914.8	2999.5	#1	PY	framboid in sediment	0.042130	0.000040	0.043023	0.000025	-9	2	
"	"	#2	"	dissemination; vein	0.042646	0.000041	"	"	3	2	
"	"	#3^{L}	CCP	Type 2 vein in sediment	0.042922	0.000041	0.043106	0.000026	2	2	
"	"	#4^{C}	"	"	0.042682	0.000042	"	"	-4	2	
"	"	#5^{R}	"	"	0.043019	0.000042	"	"	4	2	
"	"	#6^{L}	"	"	0.043087	0.000041	0.043287	0.000021	2	2	
"	"	#7^{C}	"	"	0.042775	0.000036	"	"	-5	2	
"	"	#8^{R}	"	"	0.043206	0.000036	"	"	5	2	
919.9	3016.0	#1	PY	coarse cubes in vein;	0.042486	0.000025	0.043187	0.000014	-5	2	
"	"	#2	"	some rounded corners	0.042452	0.000028	"	"	-5	2	
"	"	#3	"	in chalcopyrite	0.042519	0.000027	"	"	-4	2	
"	"	#4	"	"	0.042534	0.000028	"	"	-4	2	
"	"	#5	CCP	Type 2 vein	0.042967	0.000028	0.043175	0.000017	2	2	
"	"	#6	"	mineralisation with	0.042806	0.000028	"	"	-2	2	
"	"	#7	"	pyrite and some hematite	0.042924	0.000027	"	"	1	2	
"	"	#8	"	"	0.042990	0.000030	"	"	3	2	
962.3	3155.0	#1	GN	Type 2 (?) vein	0.043385	0.000045	0.043541	0.000023	-2	2	
"	"	#2	"	in sediment	0.043569	0.000045	"	"	2	2	
"	"	#3	"	"	0.043551	0.000044	"	"	2	2	
"	"	#4	"	"	0.043529	0.000044	"	"	1	2	
1156.3	3791.3	#1	PY	fine-grained cubes	0.042210	0.000038	0.042928	0.000018	-5	2	
"	"	#2	"	in sediment	0.042207	0.000038	"	"	-5	2	
"	"	#3	ANH	coarse nodule in sediment	0.038753	0.000039	0.038353	0.000022	17	2	
"	"	#4	"	"	0.038617	0.000043	"	"	13	3	18; 22
1157.6	3795.5	#1	PY	fine-grained cubes	0.042136	0.000036	0.042601	0.000021	1	2	
"	"	#2	"	in	0.042082	0.000041	"	"	-1	2	
"	"	#3	"	sediment	0.042138	0.000040	"	"	1	2	
"	"	#4	ANH	nodule	0.038056	0.000042	0.037887	0.000021	11	3	
"	"	#5	"	"	0.038332	0.000043	"	"	18	3	
"	"	#6	"	"	0.038068	0.000042	"	"	11	3	12; 19
1225.4	4017.8	#1	PY	porph. framboid (core)	0.042160	0.000032	0.042972	0.000019	-7	2	
"	"	#2	"	disseminated in (rim)	0.042107	0.000036	"	"	-9	2	
"	"	#3	"	nodule-rich layer (core)	0.042294	0.000033	"	"	-4	2	
"	"	#4	"	" (rim)	0.042196	0.000033	"	"	-7	2	

TABLE 2

(continued)

Depth (meters)	Depth (feet)	Crater No.	Mineral	Comments	$^{34}S / ^{32}S$ Sample	std. error (1σ)	$^{34}S / ^{32}S$ Standard	std. error (1σ)	$\delta^{34}S$ Sample	error (2σ)	Δ_{ANH-PY} (permil)
1228.8	4029	#1	PY	bedded framboids	0.042242	0.000034	0.043385	0.000020	-15	2	
"	"	#2	"	"	0.041320	0.000033	"	"	-36	2	
"	"	#3	"	"	0.041408	0.000035	"	"	-34	2	
"	"	#4	"	framboids; within CCP	0.041481	0.000033	"	"	-33	2	
"	"	#5	"	bedded framboids	0.042023	0.000033	"	"	-20	2	
"	"	#6	CCP	vein engulfing #4 PY	0.042838	0.000038	0.043328	0.000022	-4	2	
"	"	#7	"	vein; near #4 PY	0.042975	0.000049	"	"	-1	3	
"	"	#8	"	"	0.042885	0.000038	"	"	-3	2	
"	"	#9	"	vein; void of pyrite	0.042906	0.000038	"	"	-3	2	
"	"	#10	"	"	0.042879	0.000037	"	"	-3	2	
				CCP #s 6-10 Type 1 (?)							
1231.2	4036.5	#1	PY	porph. framboid (core)	0.042373	0.000042	0.042920	0.000020	-1	2	
"	"	#2	"	disseminated in (rim)	0.042151	0.000038	"	"	-6	2	
"	"	#3	"	nodule-rich layer (core)	0.042088	0.000033	"	"	-8	2	
"	"	#4	"	" (rim)	0.042203	0.000033	"	"	-5	2	
"	"	#5	"	" (core)	0.042322	0.000040	0.042972	0.000019	-4	2	
1294.5	4244.4	#1	PO	Type 1 vein in sediment	0.043088	0.000026	0.043147	0.000019	0	2	
"	"	#2	"	"	0.043018	0.000026	"	"	-2	2	
"	"	#3	"	"	0.043012	0.000030	"	"	-2	2	
1295.1	4246.3	#1	GN	Type 1 vein in sediment	0.044004	0.000044	0.043855	0.000033	5	3	
"	"	#2	"	"	0.043849	0.000040	"	"	1	3	
"	"	#3	"	"	0.043915	0.000055	"	"	3	3	
"	"	#4	SP	"	0.042498	0.000042	0.042524	0.000022	4	2	
"	"	#5	"	"	0.042692	0.000029	"	"	8	2	
1322.0	4334.5	#1	PY	disseminated cubes	0.042282	0.000037	0.042928	0.000018	-3	2	
"	"	#2	"	in sediment	0.042271	0.000036	"	"	-4	2	
"	"	#3	ANH	coarse-grained nodules	0.038301	0.000041	0.038353	0.000022	5	2	
"	"	#4	"	in sediment	0.038236	0.000039	"	"	3	2	6 - 9
1427.9	4681.3	#1	PY	stratiform in sediment	0.042822	0.000031	0.043589	0.000019	-6	2	
"	"	#2	"	"	0.043021	0.000028	"	"	-1	2	
"	"	#3	"	"	0.042948	0.000033	"	"	-3	2	
"	"	#4	CCP	Type 2 vein in sediment	0.043533	0.000031	0.043444	0.000021	9	2	
"	"	#5	"	"	0.043499	0.000032	"	"	8	2	
"	"	#6	"	"	0.043482	0.000033	"	"	8	2	
1866.6	6120	#1	PY	flow zone; coarse-grained	0.042100	0.000036	0.042683	0.000026	-2	2	
"	"	#2	"	poikiloblastic cubes	0.042132	0.000037	"	"	-1	2	
"	"	#3	"	intergrown with epidote	0.042062	0.000038	"	"	-3	2	
2098.9	6881.5	#2	PY	bedded framboidal pyrite	0.041529	0.000035	0.043319	0.000018	-30	2	
"	"	#1	"	coarse cubic overgrowth	0.042159	0.000033	"	"	-15	2	
"	"	#3	"	coarse cubic overgrowth	0.042183	0.000032	"	"	-15	2	
"	"	#4	ANH	coarse-grained, stratiform,	0.038726	0.000037	0.038662	0.000024	8	2	
"	"	#5	"	laths in	0.038721	0.000038	"	"	8	2	
"	"	#6	"	sediment	0.038579	0.000042	"	"	4	3	36; 21
2165.7	7100.5	#2	PY	bedded framboidal pyrite	0.041454	0.000032	0.043319	0.000018	-32	2	
"	"	#4	"	"	0.040764	0.000032	"	"	-48	2	
"	"	#1	"	coarse cubic overgrowth	0.042424	0.000032	"	"	-9	2	
"	"	#3	"	"	0.042386	0.000032	"	"	-10	2	
"	"	#5	"	coarse cube in sediment	0.042689	0.000033	"	"	-3	2	
"	"	#6	"	"	0.042710	0.000037	"	"	-2	2	
"	"	#7	ANH	stratiform	0.038622	0.000036	0.038662	0.000024	5	2	
"	"	#8	"	"	0.038553	0.000042	"	"	4	3	
"	"	#9	"	"	0.038525	0.000037	"	"	3	2	36; 14; 7
2302.6	7549.6	#1	PY	coarse cubes in sediment	0.043024	0.000033	0.043319	0.000018	5	2	
"	"	#2	"	"	0.042768	0.000036	"	"	-1	2	
"	"	#3	"	"	0.042859	0.000033	"	"	1	2	
2350.9	7708	#1	PY	fine-grained cube in sed.	0.042380	0.000027	0.043309	0.000016	-10	2	
"	"	#2	"	fine-grained cube in anh.	0.042502	0.000026	"	"	-7	2	
"	"	#3	"	"	0.042408	0.000027	"	"	-9	2	
"	"	#4	"	"	0.042367	0.000026	"	"	-10	2	
"	"	#5	ANH	coarse-grained stratiform	0.038625	0.000028	0.038500	0.000020	10	2	
"	"	#6	"	laths in sediment	0.038905	0.000027	"	"	17	2	
"	"	#7	"	"	0.038560	0.000028	"	"	8	2	
"	"	#8	"	"	0.038497	0.000028	"	"	6	2	
"	"	#9	"	"	0.038982	0.000028	"	"	19	2	17; 27

TABLE 2

(continued)

Depth (meters)	Depth (feet)	Crater No.	Mineral	Comments	$^{34}S/^{32}S$ Sample	std. error (1σ)	$^{34}S/^{32}S$ Standard	std. error (1σ)	$\delta^{34}S$ Sample	error (2σ)	ΔANH - PY (permil)
2360.1	7738.0	#1	PY*	framboid in sediment	0.041439	0.000027	0.043225	0.000019	-30	2	
"	"	#2	"*	"	0.041479	0.000026	"	"	-29	2	
"	"	#3	"**	pyritohedron in sediment	0.042060	0.000026	"	"	-16	2	
"	"	#4	"**	"	0.042213	0.000025	"	"	-12	2	
"	"	#5	ANH	coarse lath in sediment	0.038669	0.000028	0.038596	0.000020	8	2	
"	"	#6	"	"	0.038567	0.000031	"	"	6	2	21; 37
2481.0	8134.5	#1	PY	Type 1 fine-grained cubes,	0.041816	0.000027	0.043351	0.000017	-24	2	
"	"	#2	"	distributed parallel	0.041858	0.000027	"	"	-23	2	
"	"	#3	"	to bedding	0.041853	0.000027	"	"	-23	2	
"	"	#4*	PO	Type 1 poikilitic in sed.	0.041833	0.000033	0.042972	0.000025	-25	2	
"	"	#5**	"	massive, in veins inter-	0.042004	0.000031	"	"	-21	2	
"	"	#6	"	grown with CCP	0.041992	0.000033	"	"	-22	2	
"	"	#7	CCP	Type 1 massive, inter-	0.042230	0.000051	0.043444	0.000023	-21	3	
"	"	#8	"	grown with PO in veins	0.042172	0.000031	"	"	-23	2	
"	"	#9*	PO	as #4	0.041930	0.000032	0.042979	0.000019	-23	2	
"	"	#10**	"	as #5	0.042052	0.000027	"	"	-20	2	
2482.1	8138.0	#1	PY	fine-grained cube in anh.	0.042378	0.000024	0.043279	0.000014	-9	2	
"	"	#2	"	"	0.042326	0.000024	"	"	-11	2	
"	"	#3	"	"	0.042362	0.000024	"	"	-10	2	
"	"	#4	"	"	0.042450	0.000024	"	"	-8	2	
"	"	#5	ANH	coarse, interlocking	0.038727	0.000032	0.038516	0.000014	12	2	
"	"	#6	"	crystals; in	0.038849	0.000035	"	"	15	2	
"	"	#7	"	stratiform layer	0.038869	0.000024	"	"	16	2	
"	"	#8	"	"	0.038876	0.000030	"	"	16	2	24
2746.7	9005.5	#1	PY	fine-grained pyritohedrons	0.041502	0.000035	0.042601	0.000021	-14	2	
"	"	#2	"	in coarse anhydrite	0.041470	0.000035	"	"	-15	2	
"	"	#3	ANH	coarse, interlocking	0.038180	0.000042	0.037887	0.000021	14	3	
"	"	#4	"	crystals; in	0.038156	0.000041	"	"	13	2	
"	"	#5	"	stratiform layer	0.038123	0.000042	"	"	13	3	
"	"	#6	"	"	0.038054	0.000042	"	"	11	3	25 - 29
2747.3	9007.5	#1	PY	fine-grained cube in anh.	0.042767	0.000025	0.043293	0.000018	-2	2	
"	"	#2	"	"	0.042767	0.000025	"	"	-1	2	
"	"	#3	"	fine-grained cube in sed.	0.042878	0.000027	"	"	2	2	
"	"	#4	"	"	0.042868	0.000028	"	"	2	2	
"	"	#5	ANH	massive coarse	0.038643	0.000026	0.038744	0.000018	4	2	
"	"	#6	"	stratiform laths	0.038828	0.000027	"	"	9	2	
"	"	#7	"	"	0.038919	0.000032	"	"	11	2	
"	"	#8	"	"	0.038838	0.000042	"	"	9	2	8
2883.3	9453.4	#1	PY	very coarse cubes in vein	0.042743	0.000036	0.043154	0.000018	2	2	
"	"	#2	"	cutting diabase	0.042638	0.000035	0.042638	0.000035	0	2	
"	"	#3	"	"	0.042625	0.000035	"	"	-1	2	
"	"	#4	"	"	0.042589	0.000035	"	"	-1	2	
"	"	#5	"	"	0.042639	0.000036	"	"	0	2	
"	"	#6	"	"	0.042645	0.000036	"	"	0	2	
2883.5	9454.0	#1	PY	coarse poikilitic cubes	0.042588	0.000036	0.043195	0.000018	-2	2	
"	"	#2	"	of pyrite alligned	0.042467	0.000036	"	"	-5	2	
"	"	#3	"	parallel to the bedding	0.042423	0.000035	"	"	-6	2	
"	"	#4	"	in the sediment	0.042457	0.000035	"	"	-6	2	
"	"	#5	"	"	0.042539	0.000039	"	"	-4	2	
"	"	#6	"	"	0.042486	0.000035	"	"	-5	2	
"	"	#7	"	"	0.042556	0.000035	"	"	-3	2	
2884.3	9456.6	#1	PY	coarse-grained, cubic,	0.042000	0.000035	0.042677	0.000016	-4	2	
"	"	#2	"	euhedral pyrite in diabase	0.041948	0.000035	"	"	-6	2	
"	"	#5	"	"	0.041904	0.000036	"	"	-7	2	
"	"	#7	"	"	0.041899	0.000036	"	"	-7	2	
"	"	#10	"	"	0.041946	0.000036	"	"	-6	2	
"	"	#3	"	coarse-grained, cubic,	0.042206	0.000035	"	"	1	2	
"	"	#4	"	partially rounded	0.042175	0.000035	"	"	-1	2	
"	"	#6	"	(resorbed?) stratiform	0.042080	0.000036	"	"	-2	2	
"	"	#8	"	pyrite in sediment	0.042083	0.000036	"	"	-2	2	

TABLE 2

(continued)

Depth (meters)	Depth (feet)	Crater No.	Mineral	Comments	$^{34}S/^{32}S$ Sample	std. error (1σ)	$^{34}S/^{32}S$ Standard	std. error (1σ)	$\delta^{34}S$ Sample	error (2σ)	ΔANH - PY (permil)
2884.4	9457.0	#1	PY	coarse-grained, cubic,	0.041904	0.000036	0.042618	0.000019	-5	2	
"	"	#2	"	euhedral pyrite in diabase	0.041901	0.000036	"	"	-5	2	
"	"	#3	"	and in veins through	0.041948	0.000036	"	"	-4	2	
"	"	#4	"	fragments of sediment	0.042095	0.000043	"	"	-1	2	
"	"	#5	"	enclosed in the	0.041955	0.000041	"	"	-4	2	
"	"	#6	"	diabase	0.042003	0.000046	"	"	-3	2	
				RIVER RANCH 1							
348.3	1142	#1	PY	after sulfate	0.042850	0.000026	0.043104	0.000016	6	2	
"	"	#2	"	overgrowth on botryoidal	0.042889	0.000026	"	"	7	2	
"	"	#3	"	botroidal pyrite	0.042890	0.000026	"	"	7	2	
"	"	#4	"	cement in sediment	0.041520	0.000030	"	"	-25	2	
1491.5-1494.5	4890 - 4900	#1	PY	disseminated cube	0.043221	0.000037	0.043654	0.000016	2	2	
		#2	"	(Plate 8A; McKibben	0.043266	0.000039	"	"	3	2	
"	"	#3	"	and Elders, 1985)	0.043191	0.000035	"	"	1	2	
"	"	#4	PO	Type 1 veinlet replacing	0.043189	0.000044	0.043136	0.000026	3	2	
"	"	#5	"	PY cube	0.043255	0.000055	"	"	4	3	
"	"	#6	"	"	0.043114	0.000046	"	"	1	3	
				MAGMAMAX 11							
1046.6	3431.6	#1	PY	fine-grained cube in sed.	0.042529	0.000070	0.043691	0.000037	-15	3	
"	"	#2	"	fine-grained cube in anh.	0.042505	0.000052	"	"	-16	3	
"	"	#3	ANH	coarse laths interlayered	0.039149	0.000043	0.039177	0.000030	6	3	
"	"	#4	"	with sediment lenses	0.039438	0.000070	"	"	13	4	
"	"	#5	"	within massive anhydrite	0.039393	0.000045	"	"	12	3	22 - 28
1047.0	3432.8	#1	PY	fine-grained cube in anh.	0.042999	0.000041	0.043851	0.000034	-8	3	
"	"	#2	"	fine-grained pyritohedrons	0.043057	0.000044	"	"	-7	3	
"	"	#3	"	"	0.042846	0.000045	"	"	-11	3	
"	"	#4	ANH	coarse laths cementing	0.039235	0.000036	0.039342	0.000030	4	2	
"	"	#5	"	shale breccia	0.039395	0.000034	"	"	8	2	
"	"	#6	"	"	0.039219	0.000045	"	"	3	3	14
1050.0	3442.7	#1	PY	fine-grained cubes in	0.043006	0.000055	0.043988	0.000023	-11	3	
"	"	#2	"	sediment	0.043139	0.000044	"	"	-8	2	
"	"	#3	"	framboids in sediment	0.043063	0.000044	"	"	-10	2	
"	"	#4	"	fine-grained cube in sed.	0.043315	0.000046	"	"	-4	2	
"	"	#5	ANH	coarse laths, stratiform	0.039747	0.000042	0.039458	0.000021	14	2	
"	"	#6	"	in sediment	0.039513	0.000057	"	"	8	3	
"	"	#7	"	"	0.039670	0.000043	"	"	12	2	19
1050.1	3443	#1	PY	fine-grained framboid	0.041574	0.000042	0.042793	0.000017	-17	2	
"	"	#2	"	in sediment	0.041563	0.000057	"	"	-17	3	
"	"	#3	"	fine-grained cube	0.041712	0.000038	"	"	-14	2	
"	"	#4	"	in sediment	0.041975	0.000034	0.043242	0.000022	-18	2	
"	"	#5	"	"	0.041916	0.000037	"	"	-19	2	

PY = pyrite
CCP = chalcopyrite
ANH = anhydrite
GN = galena
PO = pyrrhotite
SP = sphalerite
porph. = coarse-grained porphyroblast, ususally ~1 mm in diameter
diss. = pyrite disseminated throughout sample
sed. = sediment
anh. = anhydrite

*Samples denoted with asterisk were analyses from craters adjacent to each other, measured several hours to days apart.

^{L}indicates the left margin of the vein, ^{C}the center, and ^{R}the right margin; analysis set 3–5 was repeated several months later by set 6–8.

ΔANH-PY: several values are obtainable depending on the pairs chosen from a given sample. If the total range possible is small, the range is given. If the total range possible is quite large, average values are given from the possible pairs.

The data from RIVER RANCH 1, 1142 ft., are from pyrites pictured in plates 6 and 7 of McKibben and Elders, 1985. Analysis #1 is in 6C; #2, #3 are in 7B, #4 is in 6A.

TABLE 3

Conventional $\delta^{34}S$ analyses of fluid and pipe scale samples

Well	Salinity*	Temperature*	$\delta^{34}S$ H_2S	mH_2S	$\delta^{34}S$ SO_4	mSO_4	$\Delta_{SO_4-H_2S}$
Fluid Samples							
S2-14-1	25.5	315	3.9	0.00059	22.1	0.00091	18.2
S2-14-3	25.7	317	0.1	—	18.8	0.00173	18.7
DR-1	23.0	299	−0.9	0.00045	17.2	—	18.1
DR-3	23.0	299	0.5	0.00045	19.4	0.00072	19.5
	23.0	299	−0.8				
DR-6	22.8	304	3.1	—	21.1	0.00036	18.0
EL-14	25.7	318	3.4	—	21.4	0.00088	18.0
EL-4[2]	22.5	313	4.3	0.00124	—	0.00076	
I1-13[3]	1.3	200	—	—	10.0	—	
CW-1	9.4	250	—	—	15.8	—	
	12.4	280	—	—	[2]11.4	—	
RR-3	25.0	312	−1.4	0.00136	—	0.00078	
MM-10	21.4	297	0.3	—	—	0.00174	
IW-1[3]	20.0	301	7.3	0.00084	—	0.00069	
Pipe Scales							
SP-1[4]	24.9	305	0.2	—	—	—	
HD-1[4]	25.8	320	1.1	—	—	—	
	25.8	320	2.6	—	—	—	
	25.8	320	1.2	—	—	—	
SC-3[4]	unknown	unknown	—	—	5.6	—	
Mudpot	unknown	≈15	−29.8	—	—	—	

*Pre-flash reservoir fluid salinity (wt percent TDS) corrected for steam loss. Reservoir fluid temperature (°C) based on Na—K—Ca geothermometer and downhole logging (Williams and McKibben, 1989).

[2]Well-bore mixing of fluids from more than one flow-zone was likely.

[3]Short flow duration may have prevented complete clean-out of drilling fluids from well.

[4]From White (1968) and written communication, 1986.

and deep hypersaline brines are given in McKibben and others (1987), McKibben, Andes, and Williams (1988), and Williams and McKibben (1988).

H_2S and SO_4 were collected from flow-line ports during individual well flow tests lasting 1 to 10 days. At the flash temperatures common for SSGS well flow tests (250°–300°C), we assumed that H_2S was partitioned quantitatively into the steam phase and that SO_4 remained quantitatively in the flashed brine. Fluid from steam ports was passed through cooling coils immersed in an ice bath. The resulting mixture of steam condensate and noncondensable gas was passed through two traps in series, each consisting of fritted glass dispersion tubes immersed in 1 l graduated cylinders containing solutions of Cd or Zn salts. This arrangement yielded finely-divided gas bubbles which ascended a relatively long fluid path length, causing the H_2S to precipitate as CdS or ZnS. With Cd solutions, rapid precipitation of CdS in the traps indicated that removal of H_2S was quantitative. With Zn solutions, however, sluggish colloidal ZnS precipitation occurred, and total S yields were ≈10 percent of those

obtained with Cd solutions. There was no difference in the sulfur isotopic compositions obtained by using either type of solution.

Flashed brine was collected in 6 l polyethylene bottles from cooling coils attached to brine ports or was collected directly from the Wier box. The brine was diluted and acidified in the field to retard hydroxide and silica precipitation. After filtering the treated brine in the laboratory, $Ba(NO_3)_2$ was added to precipitate aqueous SO_4 as $BaSO_4$ for $\delta^{34}S$ analysis.

One sample of H_2S was collected from a cold surface CO_2 mudpot in the northeastern SSGS (fig. 2) by placing an inverted teflon funnel over the mudpot and drawing the gas into the two-stage trap with a small hand-pump.

All CdS and ZnS precipitates were converted to Ag_2S in the laboratory prior to $\delta^{34}S$ analysis, using the methods of Thode, Monster, and Dunford (1961), and Sasaki, Arikawa, and Folinsbee (1979). Ag_2S and $BaSO_4$ were analyzed by the United States Geological Survey using conventional techniques as described above.

RESULTS

Sulfur isotope analytical results are presented in permil relative to the Canyon Diablo troilite standard in tables 1 and 3 (conventional data) and 2 (SHRIMP data) and are summarized in figures 3 and 4, respectively. 2σ errors quoted for conventional data are ± 0.1 permil, whereas those for SHRIMP data are generally ± 2 permil. The mean values and ranges for both data sets generally are in excellent agreement. However, a much wider range in $\delta^{34}S$ is exhibited by the SHRIMP analyses of pyrite in sediments. Many of the conventional $\delta^{34}S$ analyses of sedimentary pyrite were of samples of coarse cubes ("porphyroblasts") collected from drill cuttings described by McKibben and Elders (1985). In contrast, the SHRIMP analyses were conducted on all pyrite types (coarse cubes and fine stratiform layers) observed in sediments in the S2-14 cores. Consequently, the SHRIMP analyses provide a more complete and accurate record of the total range in $\delta^{34}S$ of all types of sedimentary pyrite than the limited number of conventional analyses.

The primary database on SSGS wells is in units of feet, so specific samples are identified by a code comprised of well name and depth in feet (S2-14 7100.5). However, tables 1 and 2 give solid sample depths in both meters and feet, and all discussions and illustrations involving depth are given in both units.

Stratiform Gypsum and Anhydrite

Sulfate minerals in the deltaic-lacustrine SSGS host sediments range from disseminated mm- to cm-sized crystals and nodules in mudstones to 0.6 m-thick stratiform bedded accumulations of gypsum and anhydrite (McKibben, Williams, and Okubo, 1988; Osborn, ms; Osborn, McKibben, and Williams, 1988; Herzig, Mehegan, and Stelting, 1988). $CaSO_4$ textures are indicative of formation in an upward-

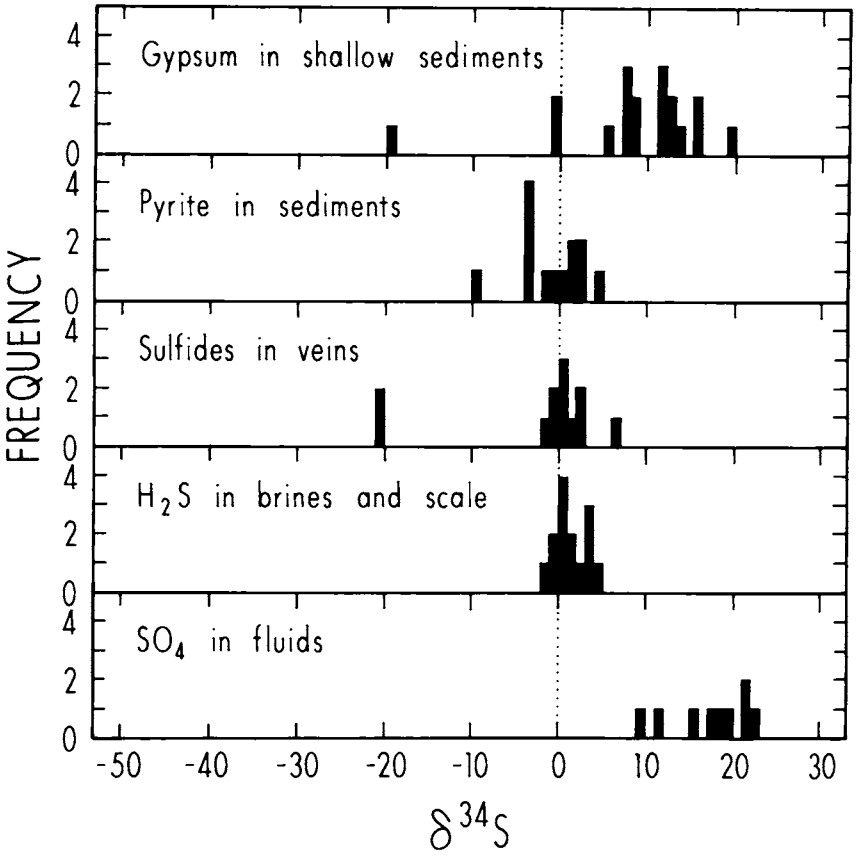

Fig. 3. Histograms of conventional sulfur isotope values listed in tables 1 and 3.

regressional continental playa-sabkha environment. The $\delta^{34}S$ data for these sulfates lie chiefly between 0 and 20 permil with a mean of 10 permil.

In unconsolidated sediments at depths less than about 610 m (2000 ft), gypsum is the dominant sulfate mineral, occurring as nodules and coarse radial crystal sprays (up to 1 cm in diam). Conventional $\delta^{34}S$ values of such material (fig. 3; table 1) show a wide range from −0.7 to 19.8 permil and one anomalous value of −19.7 permil.

Deeper sulfate occurrences consist exclusively of anhydrite, as flattened nodules (up to 3 cm), stratiform gypsum pseudomorphs (up to 2 cm), and massive to bedded hornfelsic material (1 cm–0.6 m in thickness) within lithified and metamorphosed sediments. SHRIMP $\delta^{34}S$ values for anhydrite range from 3 to 19 permil (figs. 4 and 5; table 2). Aside from the one extremely low $\delta^{34}S$ value in a shallow gypsum sample,

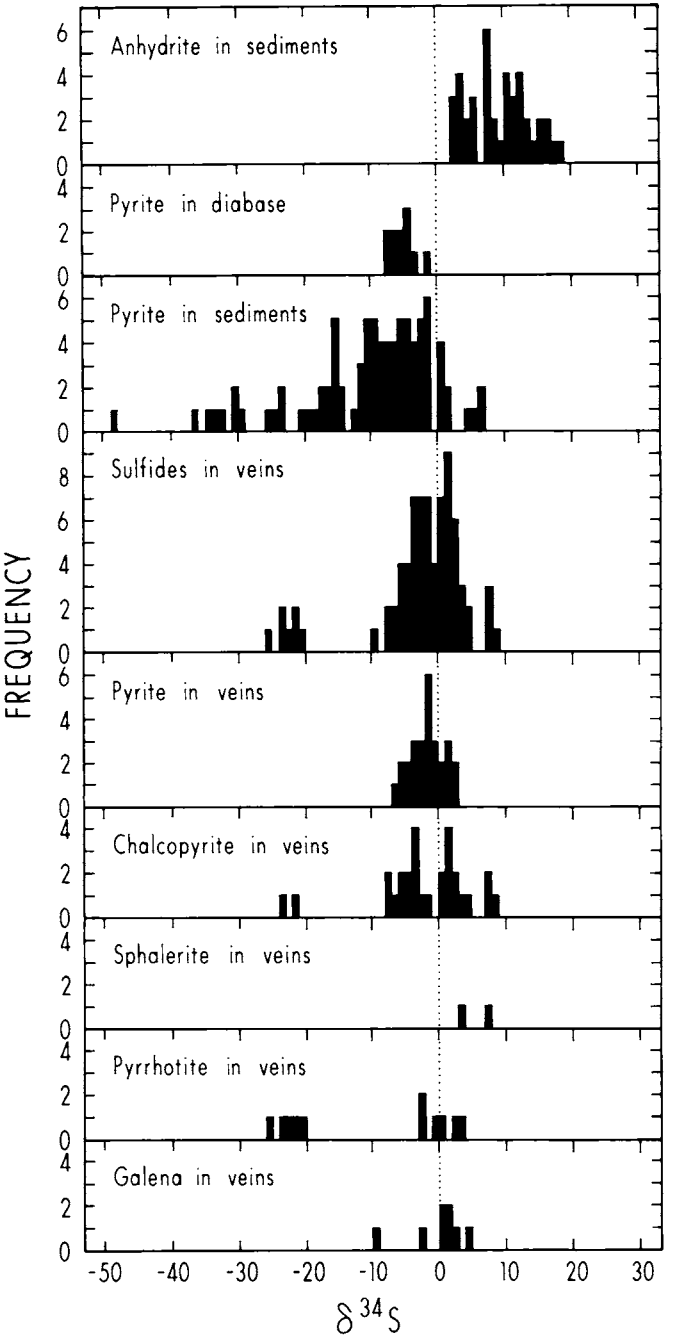

Fig. 4. Histograms of SHRIMP sulfur isotope values listed in table 2.

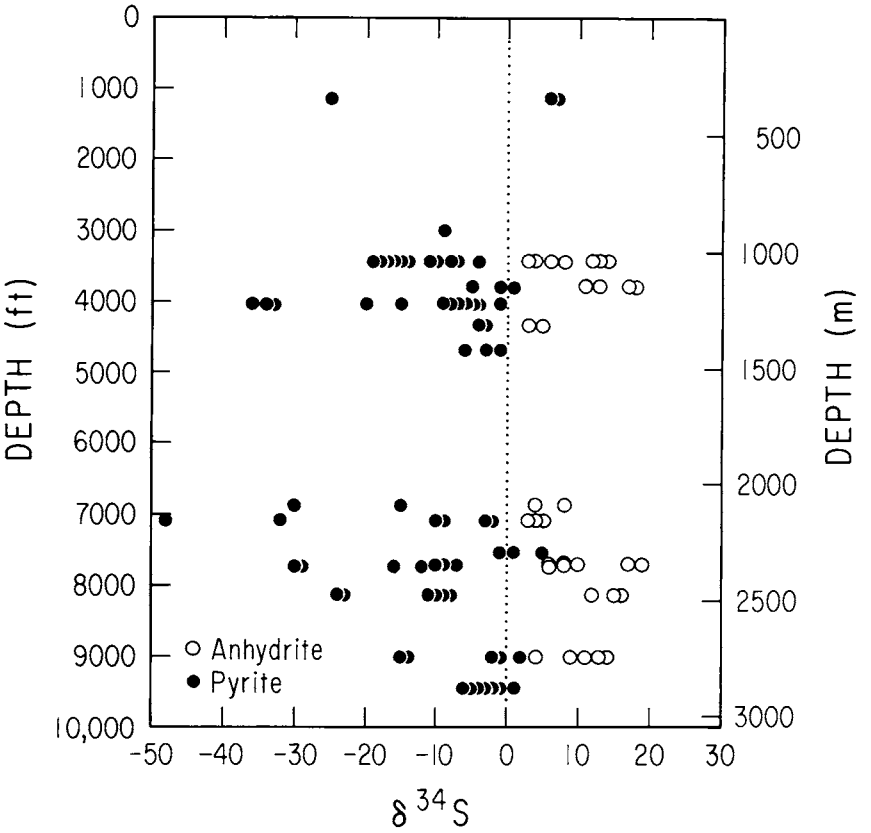

Fig. 5. SHRIMP $\delta^{34}S$ values of sedimentary pyrite and anhydrite plotted against depth (data from table 2).

the ranges of the anhydrite and gypsum $\delta^{34}S$ values are almost indistinguishable. However, the SHRIMP analyses do show considerable microscopic variation within individual anhydrite samples, such as 6 to 19 permil in S2-14 7708 (fig. 6A; table 2), 4 to 11 permil in S2-14 9007.5 (fig. 6B; table 2), and 6 to 13 permil in MM-11 3431.6 (table 2). Within S2-14 7708 the 13 permil range in $\delta^{34}S$ occurs over a distance of only 0.25 mm (fig. 6A).

Other Salton Trough Evaporites

Material from the Durmid Hills, located immediately east of the Salton Sea near the San Andreas fault (fig. 1) (Babcock, 1974), included bedded gypsum from outcrops (11.6 permil, table 1) as well as thenardite (Na_2SO_4) from localized pods and lenses (0.7 permil, table 1) in the Bertram Mine (Morton, 1977). Extensive Miocene gypsum and anhy-

drite beds in the U.S. Gypsum Mine in the Fish Creek Mountains (Morton, 1977; Ver Planck, 1952; Winker, ms), located at the southwest edge of the Salton Trough (fig. 1), were found to have $\delta^{34}S$ values of 21.1 permil (table 1).

Pyrite in Sediments

Pyrite typically occurs as disseminated stratabound cubes (5–100 μm) and rare pyritohedra (up to 0.1 mm) and as patchy to framboidal fine-grained (5–50 μm) masses and stratiform layers and lenses. Sedimentary pyrite rarely makes up more than one volume percent of a core sample of sedimentary rock. In general the pyrites are isotopically light, ranging from −48 to 6 permil (figs. 3 and 4; tables 1 and 2). The relationship between isotopic composition and morphology is complex. In many cases the diagenetic pyrite exhibits several morphologies, which may or may not display evidence of temporal relationships, and several isotopic populations. Layers can contain scattered fine-grained masses and cubes that are isotopically similar (fig. 6C; MM-11 3443.0, table 2). Pyrite crystals (up to 1 mm in diam) with patchy to framboidal cores and cubic rims may likewise be relatively homogeneous in isotopic composition (S2-14 4036.8, table 2). There can also be strong isotopic heterogeneity (−33 to −15 permil) within a uniform fine-grained morphology (fig. 6D; S2-14 4029, table 2). Some examples exhibit both isotopic and morphologic heterogeneity: fine-grained patchy to framboidal pyrite (−48 to −30 permil), overgrown and surrounded by coarse-grained cubic pyrite (−15 to −9 permil) (fig. 7A and B; S2-14 6881.5 and 7100.5, table 2). A third of the stratiform pyrite samples we probed contained similar bimodal populations of sulfur isotopic compositions as well as morphologies (table 2). One sample (fig. 7B; S2-14 7100.5, table 2) had two morphological pyrite types and three easily distinguishable isotopic groups of $\simeq -3$, $\simeq -10$, and $\simeq -40$ permil, separated spatially by only 0.25 mm. The isotopically heavy pyrite cube contains tiny chalcopyrite inclusions and may be hydrothermal in origin (see below).

All SHRIMP $\delta^{34}S$ data from pyrite in sediments have been summarized and plotted versus depth in figure 5. While there is a considerable range in $\delta^{34}S$ values overall and within many individual samples, there is no obvious relationship between $\delta^{34}S$ value and depth in the sedimentary column.

Sedimentary Anhydrite-Pyrite Isotopic Fractionation

The apparent sulfur isotopic fractionation between intergrown sedimentary anhydrite and pyrite ($\Delta_{anh\text{-}py}$) can be quite variable (table 2). In some samples there are several generations of pyrite whereas the anhydrite seems isotopically homogeneous, giving rise to several possible Δ values in a single sample (S2-14 7100.5, table 2). Alternatively, some anhydrite appears to be isotopically zoned, whereas the pyrite may be relatively uniform in isotopic composition (fig. 6A; S2-14 7708, table 2). In many samples, however, Δ is homogeneous throughout, whether between anhydrite and immediately adjacent pyrite or between anhy-

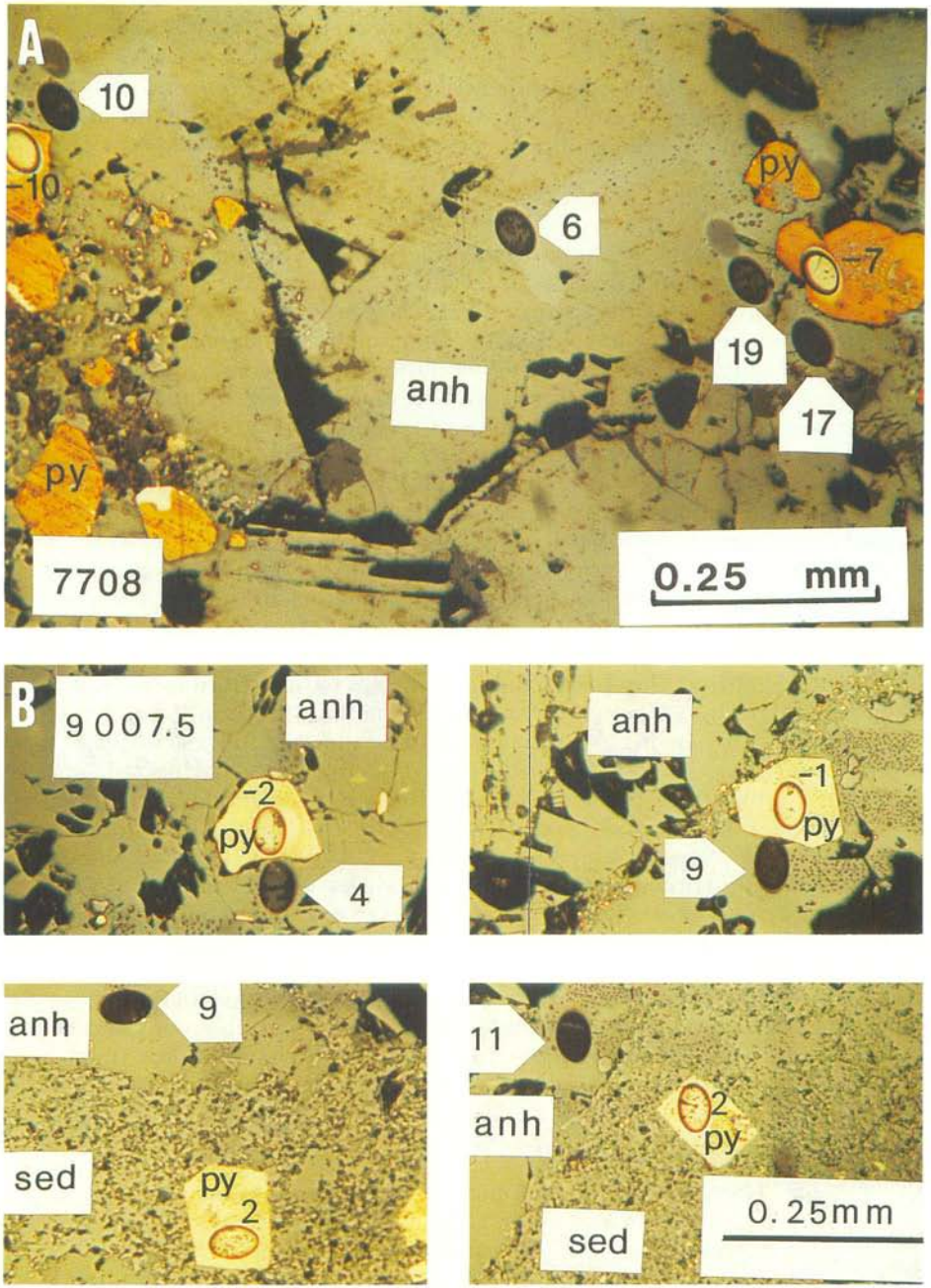

Fig. 6. Photomicrographs of representative textures examined by SHRIMP microanalysis (anh = anhydrite, py = pyrite, cpy = chalcopyrite, sed = sediment). Carbon coating causes some distortion of colors in reflected light. Numbers within arrows next to SHRIMP craters are $\delta^{34}S$ values in permil. (A) Stratiform anhydrite and pyrite (S2-14 7708). Note 13 permil variation in $\delta^{34}S$ for anhydrite over distance of only 0.25 mm. (B) Composite of stratiform anhydrite and pyrite intergrowths (S2-14 9007.5). Note that Δ values are relatively constant (6–10 permil), irrespective of whether pyrite is within anhydrite or detrital sediment.

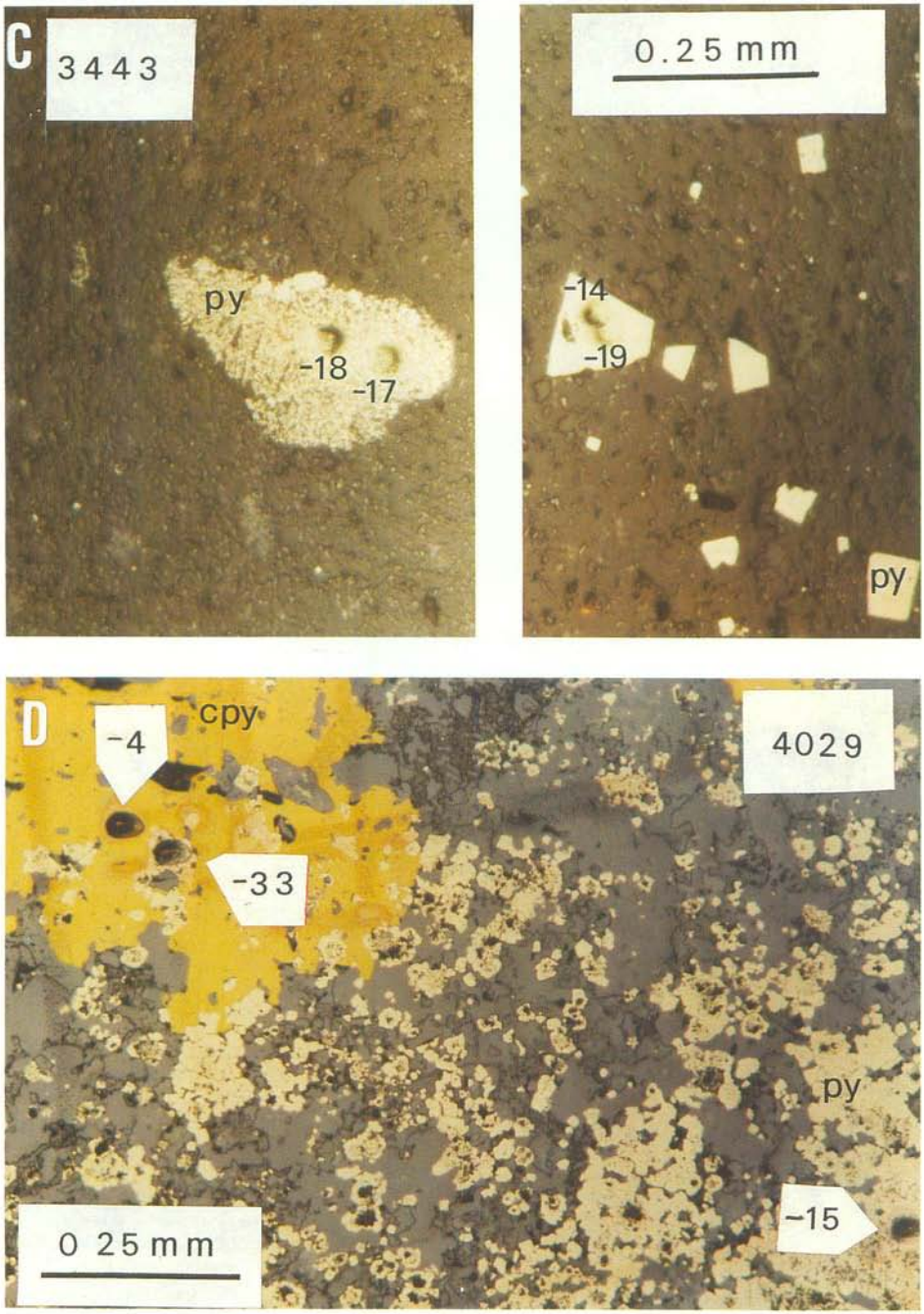

Fig. 6 (continued) (C) Composite of sedimentary pyrite, fine-grained mass (left) and euhedral crystals (right), having identical isotopic compositions (MM-11 3443.0). (D) Fine-grained framboidal sedimentary pyrite (−33 permil) completely enveloped by isotopically distinct vein chalcopyrite (−4 permil) in upper left corner.

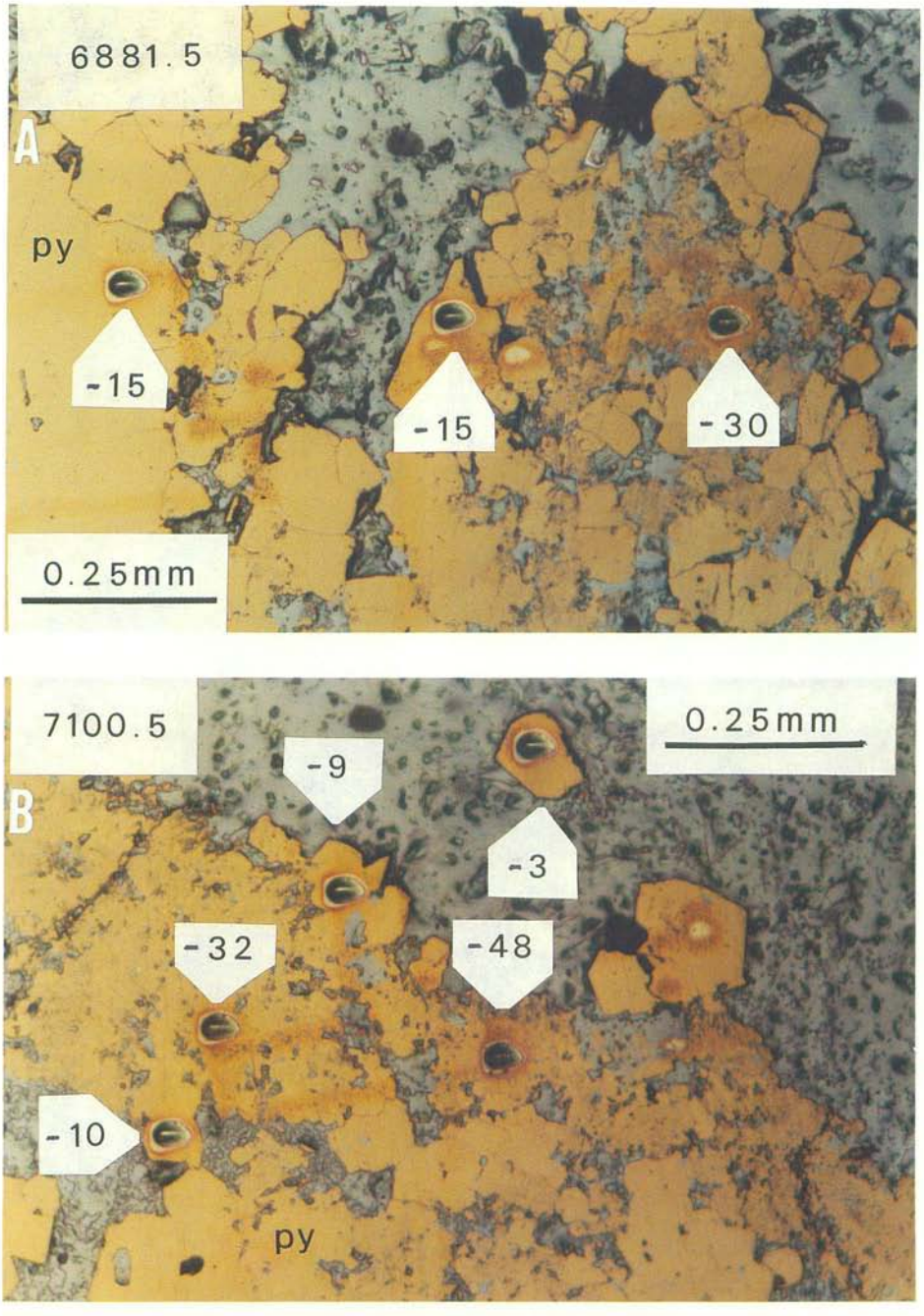

Fig. 7. Photomicrographs of representative textures examined by SHRIMP microanalysis (py = pyrite, cpy = chalcopyrite; po = pyrrhotite). Carbon coating causes some distortion of colors in reflected light. Numbers within arrows next to SHRIMP craters are $\delta^{34}S$ values in permil. (A) Stratiform pyrite in sediment showing fine-grained patchy pyrite (−30 permil) overgrown and surrounded by heavier coarse euhedral pyrite (−15 permil) (S2-14 6881.5). (B) Stratiform pyrite in sediments showing fine-grained patchy pyrite (~−40 permil) overgrown and surrounded by heavier coarse euhedral pyrite (~−10 permil; note also isolated euhedral crystal of hydrothermal (?) pyrite (−3 permil) (S2-14 7100.5).

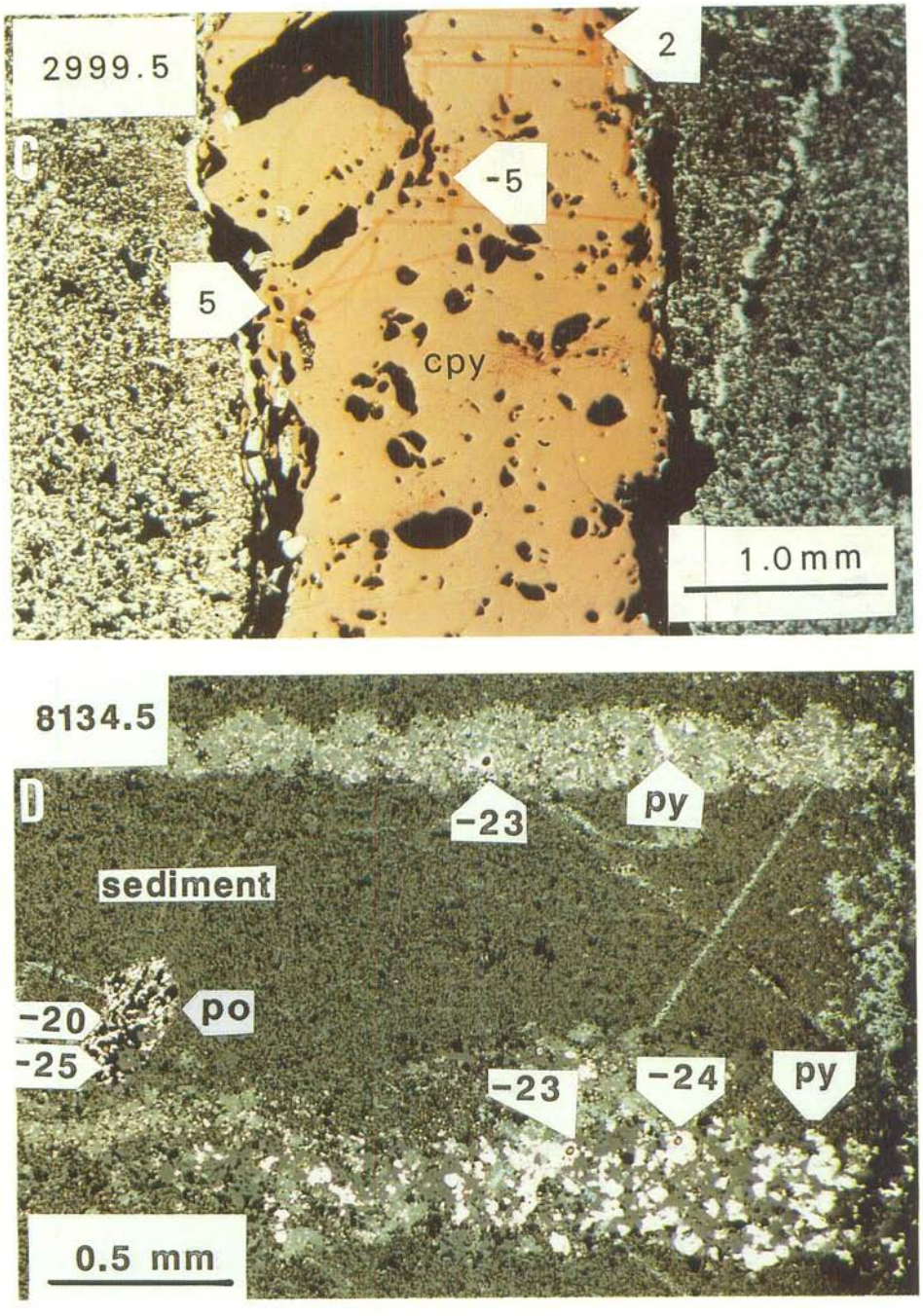

Fig. 7 (continued) (C) Monomineralic segment of type 2 vein showing symmetric isotopic zoning in chalcopyrite (S2-14 2999.5). (D) Stratiform pyrite with isotopic values (~−23 permil) identical to immediately adjacent type 1 vein pyrrhotite (~−22 permil) (S2-14 8134.5). The stratiform pyrite is clearly secondary, intergrown with authigenic silicates along bedding planes.

drite and pyrite isolated in nearby sediment (fig. 6B; S2-14 9007.5, table 2). The plot of $\Delta_{anh\text{-}py}$ versus depth is as complicated as these many examples, and no apparent trend can be found in the data (fig. 8).

Pyrite in Igneous Rocks

An altered diabase sill and its lower contact zone were cored at a depth of 2.9 km in the well S2-14 (Elders, 1987; Herzig and Elders,

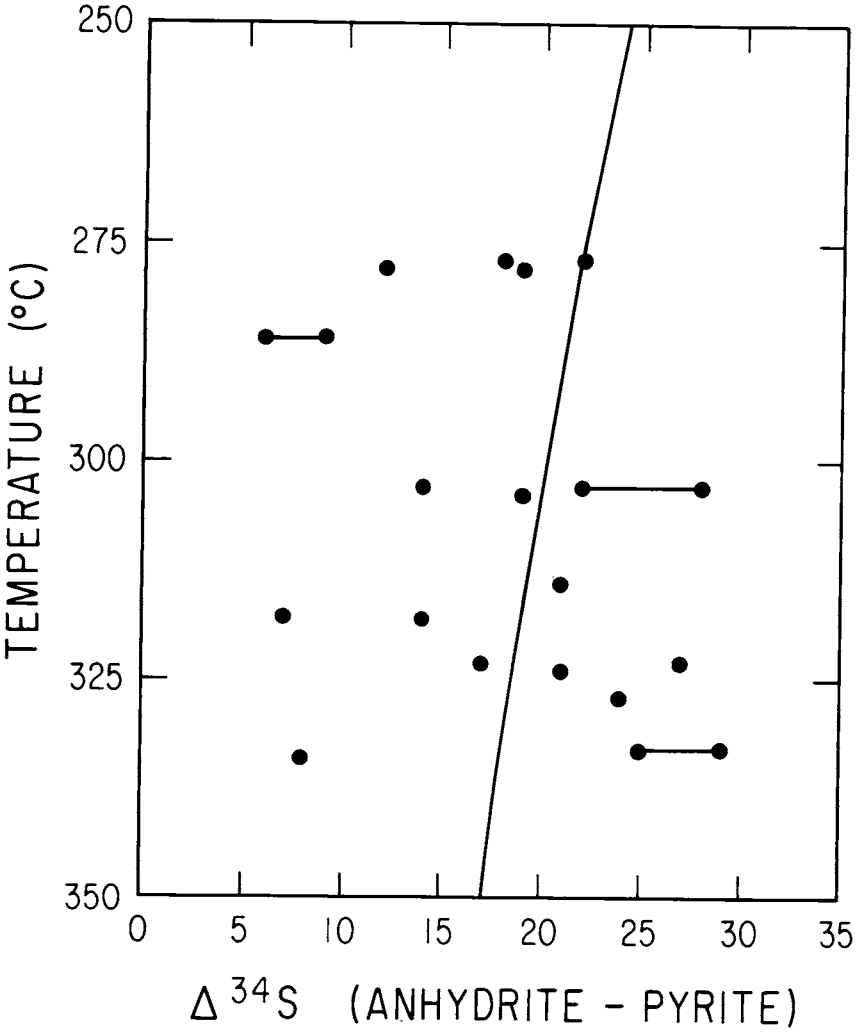

Fig. 8. Plot of apparent isotopic fractionation ($\Delta_{anh\text{-}py}$) between intergrown sedimentary anhydrite and pyrite in S2-14 and MM-11 (table 2) against mearured downhole temperature (°C) (Sass and others., 1988; McKibben, Andes, and Williams., 1988). Horizontal lines denote samples in which a range of $\Delta_{anh\text{-}py}$ values was observed. Curve is equilibrium $SO_4 - H_2S$ isotopic fractionation from Ohmoto and Lasaga (1982).

1988). Although the dense main mass of the sill is devoid of any disseminated sulfides, brecciated metasediments within the contact zone are intruded by stringers of diabase containing abundant euhedral pyrite crystals up to 1 mm across. Figure 9A shows the complex contact zone of the sill. Pyrite associated with the diabase stringers and contact metasediments occurs in three forms. (1) Pyrite occurs within the diabase stringers as concentrated bands of euhedral crystals which are generally conformable to, but sometimes transgress, the stringer-metasediment contacts (fig. 9A and B). This intrasill pyrite *replaces* plagioclase phenocrysts and groundmass in the diabase (fig. 9B) and has $\delta^{34}S$ values from -7 to -1 permil (fig. 4 and 9B; S2-14 9456.6 and 9457.0, table 2). (2) Pyrite cubes occur as random to stratiform disseminations and bands within the metasediments (fig. 9C), which in some cases transgress diabase-metasediment contacts. This pyrite has $\delta^{34}S$ values from -6 to 1 permil (S2-14 9454.0 and 9456.6, table 2), similar to the range for intrasill pyrite. In S2-14 9456.6 both intrasill (-7 to -4 permil) and stratiform (-2 to 1 permil) pyrites occur within millimeters of one antoher, exhibiting distinct sulfur isotopic ranges and suggesting that there may actually be two populations. (3) Pyrite is also found as coarse-grained cubes in hydrothermal veins that clearly cut and post-date the main mass of the diabase sill. This vein pyrite has $\delta^{34}S$ values from -1 to 2 permil (S2-14 9453.4, table 2), similar to those of pyrites in other hydrothermal veins (see below).

No recognizable silicic intrusions were penetrated by well S2-14. Robinson, Elders, and Muffler (1976) reported possible subsurface silicic rocks in drill cuttings from other wells, but they were altered to secondary chlorite, epidote, amphibole, and pyrite. They also contained much higher K_2O, CaO, and FeO contents and lower SiO_2 and Na_2O contents than the surface domes, reflecting intense alteration by the geothermal brines. Our reflected-light examination of several of the thin sections of surface rhyolite domes prepared by Robinson, Elders, and Muffler (1976) yielded no evidence of sulfides.

Vein Sulfate and Sulfide

Vein mineralization in the SSGS is typically accompanied by chlorite-epidote alteration and depletion of ^{18}O in the host sediments (Sturtevant and Williams, 1987) and is most abundant in the depth interval 610–1524 m (2000–5000 ft). Both type 1 (early pyrrhotite-bearing) and type 2 (modern pyrite-epidote-hematite-bearing) veins of McKibben, Andes, and Williams (1988) have been sampled for this study. With the exception of one isotopically light type 1 vein, vein minerals have a fairly limited range of sulfur isotopic compositions (-9 to 9 permil with a mean of $\simeq 0$ permil, figs. 3 and 4) with no significant correlation between isotopic composition and depth in the hydrothermal system (fig. 10). The anomalous type 1 vein (S2-14 8134.5, table 2) occurs near the base of a thick, impermeable shale unit, and sulfide mineralization is distributed in a vertical fracture as well as along bedding planes. Though the vein chalcopyrite and pyrrhotite and

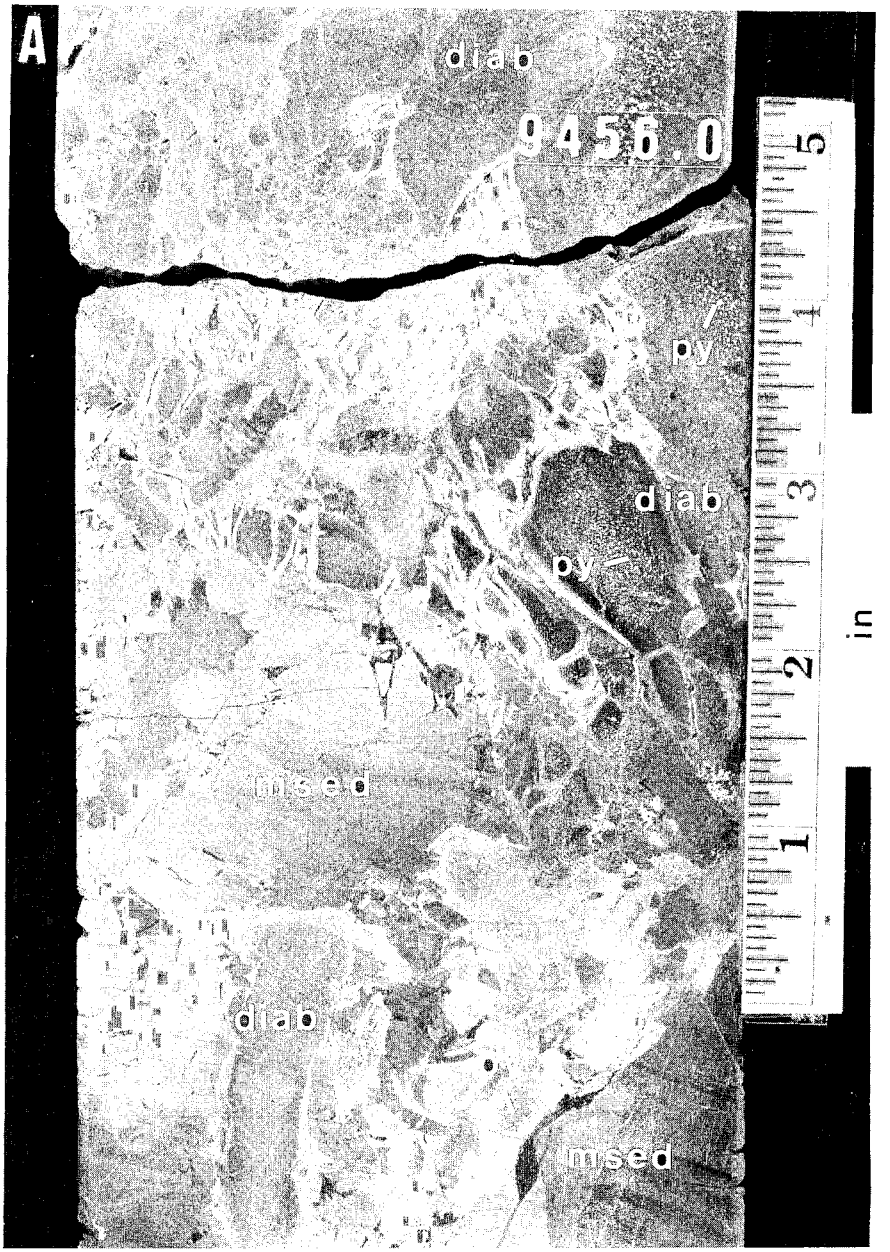

Fig. 9. Diabase sill-metasediment contact zone, 2882 m (9456 ft) depth, S2-14 well. (A) Contact zone showing diabase stringers (diab) in brecciated metasediment (msed) with associated pyrite (py).

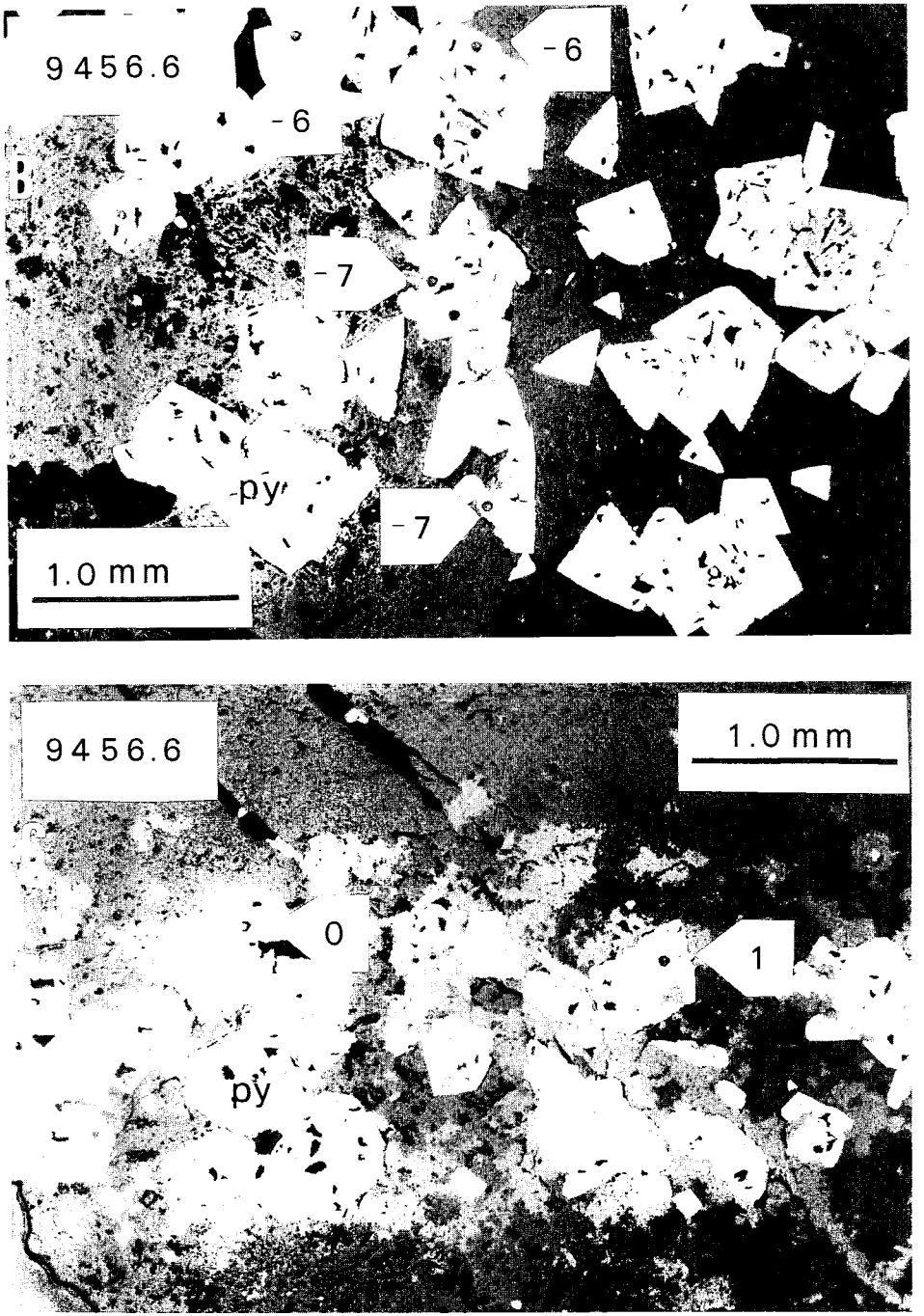

Fig. 9 (continued) (B) Photomicrograph of intrasill pyrite (py) replacing plagioclase phenocrysts and groundmass in diabase stringer (S2-14 9456.6). (C) Photomicrograph of stratiform pyrite (py) in metasediments (S2-14 9456.6). Labelled arrows next to craters in (B) and (C) show results of SHRIMP $\delta^{34}S$ microanalysis in permil.

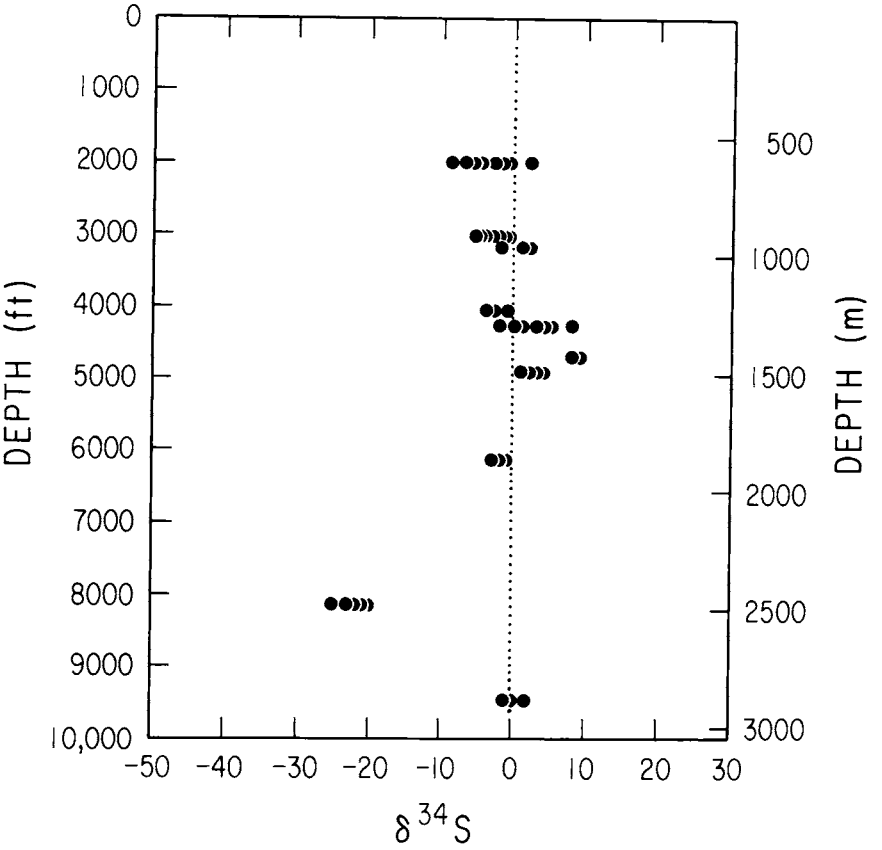

Fig. 10. Plot of SHRIMP $\delta^{34}S$ values for vein sulfides (table 2) against depth.

stratiform pyrite and pyrrhotite in this sample occur within coarse-gained and altered portions of the wall-rock, the bulk of the shale has not undergone significant ^{18}O depletion (Sturtevant and Williams, 1987), and this mineralization may represent only a local event. Regardless of vein type or time of formation, veins having several sulfides intergrown generally show the expected order of ^{34}S enrichment (Ohmoto and Rye, 1979) with pyrite exhibiting the highest $\delta^{34}S$ values and galena the lowest (table 2).

Anhydrite.—Vein anhydrite is relatively rare in the SSGS (McKibben and Elders, 1985; McKibben, Andes, and Williams, 1988). Some occurrences of fracture-filling anhydrite may represent locally dissolved and reprecipitated metaevaporitic material rather than hydrothermally-introduced vein sulfate (McKibben, Williams, and Okubo, 1988). SHRIMP analyses of such material from the well MM-11 yielded a $\delta^{34}S$

range from 3 to 8 permil (MM-11 3432.8, table 2). Three samples of apparent vein anhydrite in drill cuttings from MM-2 were analyzed conventionally and fall in a narrow range from 9.5 to 9.7 permil (table 1).

Pyrite.—Pyrite was generally the earliest sulfide phase precipitated in veins (McKibben and Elders, 1985; McKibben, Andes, and Williams, 1988) and is typically found as 5 μm to 3 mm cubic crystals. It occurs in both type 1 and 2 veins, associated with other sulfides and/or oxides and in some cases locally as the only vein sulfide (table 2). Conventional $\delta^{34}S$ values of "pyrite in reservoir rocks" (presumably vein material) reported by White (1968) from the wells IID-1 and SP-1 range narrowly from -1.4 to 3 permil (table 1).

Microanalysis has shown that individual pyrite crystals or veins are not isotopically zoned. $\delta^{34}S$ values range from -6 to 3 permil (fig. 4; table 2), with a mean near -2 permil. There is no clearcut distinction between the isotopic composition of pyrite in type 1 and type 2 veins, except for the stratiform, possibly hydrothermal, pyrite associated with the anomalously ^{34}S-depleted type 1 vein sulfides of S2-14 8134.5 (fig. 7D; tables 1 and 2).

Cubes of pyrite up to several mm across occur in porous epidote-rich vein fragments that were ejected from the well-bore during the first SSSDP flow-test at 1898 m (6227 ft) in the well S2-14, (Charles and others, 1988; Elders and Sass, 1988). $\delta^{34}S$ values for this pyrite ($\simeq -2$ permil, table 2) are significantly depleted in ^{34}S relative to the H_2S sample collected during this flow test (3.9 permil, table 3). However, a later flow test from this well (which may have sampled a different fracture zone) yielded more S^{34}-depleted H_2S (0.1 permil, table 3). Because the porous ejecta represent mineral assemblages in open fractures that are interacting with the modern geothermal fluids, the pyrite in these samples must represent some of the most recently-precipitated sulfides in the SSGS.

In situ analyses have demonstrated that in those samples containing intergrown hydrothermal and sedimentary sulfide (fig. 6D and 7B; S2-14 4029 and 7100.5, table 2), the hydrothermal sulfide does not have isotopic values shifted significantly toward the very light sedimentary pyrite compositions.

Chalcopyrite.—Chalcopyrite in veins ranges from massive anhedral material to isolated euhedral crystals up to 1 cm in diameter (McKibben and Elders, 1985; McKibben, Andes, and Williams, 1988). While conventional $\delta^{34}S$ values range narrowly from 0.1 to 1.6 permil (table 1), considerable isotopic variation has been found (-23 to 9 permil, table 2) using SHRIMP, though the mean of the data still lies near 0 permil (fig. 4). One sample of chalcopyrite from the anomalous type 1 vein has a $\delta^{34}S$ value of -23 permil while the rest of type 1 and all the type 2 chalcopyrites have isotopic compositions between -7 and 9 permil (fig. 4). Many samples of chalcopyrite are isotopically homogeneous, even though some portions of the vein material enclose diagenetic pyrite of

radically different isotopic composition (fig. 6D; S2-14 4029, table 2). One monomineralic chalcopyrite vein, however, shows significant isotopic zoning of 10 permil within the space of 1 mm (fig. 7C; S2-14 2999.5, table 2). The zoning is roughly symmetrical with higher values on the margins (2–5 permil) and lower values in the middle (−5 permil). The zoning was reproduced to within 1 permil in two analytical sessions months apart (table 2).

Sphalerite.—Conventional $\delta^{34}S$ values for two samples of vein sphalerite in the well RR-1 are ≃1 permil (table 1). SHRIMP $\delta^{34}S$ values for one sample of vein sphalerite from S2-14 4246.3 are significantly higher: 4 and 8 permil (fig. 4; table 2).

Pyrrhotite.—Pyrrhotite is characteristic of the reduced type 1 veins (McKibben and Elders, 1985; McKibben, Andes, and Williams, 1988). Pyrrhotite from the anomalous S2-14 8134.5 vein has $\delta^{34}S$ values of ≃−22 permil (fig. 7D) consistent with those of the associated pyrite and chalcopyrite (figs. 3 and 4; tables 1 and 2). Other occurrences of vein pyrrhotite have $\delta^{34}S$ values from −2 to 6 permil (fig. 4: S2-14 8398, table 1; S2-14 4244.4 and RR-1 4895, table 2) which are closer to the mean value for all vein sulfides (fig. 4).

Galena.—In situ $\delta^{34}S$ values for three samples of vein galena range widely from −9 to 5 permil (fig. 4, table 2) without regard for vein type; the values generally increase with depth.

Fluid Precipitates and Pipe Scales

Fluid precipitates and pipe scales are considered jointly, because both represent samples of H_2S and SO_4 derived from the modern geothermal fluids. Figure 11 shows $\delta^{34}S$ values of H_2S and SO_4 samples precipitated from the fluids plotted versus reservoir temperature and fluid salinity. Similar means of $\delta^{34}S$ values are found for sulfide scale (1.3 permil) and H_2S (1.8 permil) from the deep hypersaline brines (table 3; fig. 3). Some isotopic variability is evident in samples collected about an hour apart during flow-testing of the well DR-3 (Δ = 1.3 permil, table 3) and 30 months apart in the well S2-14 (Δ = 3.8 permil, table 3).

The total range (6–22 permil, table 3) in $\delta^{34}S$ values for sulfate scale and aqueous SO_4 from all geothermal fluids sampled is significantly greater than that found for H_2S. The highest values (17–22 permil) are from the deep hypersaline brines (>20 wt percent TDS, fig. 11B), and all but one of the lower $\delta^{34}S$ values (10–16 permil) are from shallow lower-salinity fluids (<10 wt percent TDS, fig. 11B) or from well-bore mixtures of low-salinity and hypersaline fluids produced from multiple flow-zones over large uncased intervals in wells (CW-1, table 3). One sample of sulfate scale (5.6 permil, SC-3 table 1) reported by White (1986, personal commun.) is from a flow-test of unknown reservoir temperature and salinity and is not included in figure 3. The $\delta^{34}S$ values of SO_4 generally appear to increase with increasing salinity and temperature as the fluid interface is approached and crossed (fig. 11), but there

are exceptions: SO_4 from a shallow low-salinity flow-zone, sampled early in the drilling of well CW-1, is 4 permil heavier than the SO_4 from a slightly more saline well-bore mixture produced later from this well.

Comparison of the isotopic compositions of aqueous SO_4 and anhydrite (figs. 3 and 4) shows that the maximum $\delta^{34}S$ value of the SO_4 from the deep hypersaline brines exceeds that of any anhydrite found by 3 permil and is enriched in ^{34}S relative to the mean anhydrite value (10 permil) by 12 permil.

Aqueous SO_4-H_2S isotopic fractionation.—Paired samples of H_2S and SO_4 in the hypersaline brines were collected during six flow-tests of five wells (table 3). The reservoir temperatures of all six brines fell within 299° to 318°C, and differences in isotopic composition between H_2S and SO_4 were remarkably consistent at 18 to 19 permil.

Surface Mudpot

Bubbling mudpots in the CO_2 field on the northeast margin of the SSGS (fig. 2; Muffler and White, 1968) exhibit ambient temperatures: only one produced sufficient H_2S for isotopic analysis. Sediment within this mudpot was darker in color and contained more organic matter than that within other mudpots. The H_2S from the mudpot had the lowest $\delta^{34}S$ value (−29.8 permil, table 3) of any H_2S collected in our study.

INTERPRETATION AND DISCUSSION

Isotopic Equilibration of Pyrite and Anhydrite

It might be anticipated that, whatever their initial isotopic compositions, intergrown diagenetic sulfate and sulfide in the SSGS sediments might approach a new equilibrium distribution of ^{34}S if recrystallization occurred during burial and metamorphism, and that the degree of approach would correlate with increased depth of burial and temperature. Gypsum dehydrates to anhydrite at depths of 225 to 250 m (80°–105°C) in the SSGS (Osborn, ms: Osborn, McKibben, and Williams, 1988). The presence of dehydration waters as well as later hydrothermal brines could enable such isotopic re-equilibration by providing a medium for isotopic exchange during recrystallization. $\Delta_{anhydrite\text{-}pyrite}$ values are listed in table 2 and are plotted versus present measured downhole temperature in figure 8. There is no evidence for the deep SSGS metasediments having been exposed to temperatures markedly greater than those presently measured downhole. The comparison of measured $\Delta_{anhydrite\text{-}pyrite}$ values with $\Delta_{SO_4\text{-}H_2S}$ expected at equilibrium in hydrothermal fluids (fig. 8) illustrates that there has been no shift toward equilibrium isotope partitioning between sulfate and sulfide in the Pleistocene and younger sediments at the upper greenschist to lower amphibolite facies (Cho, Liou, and Bird, 1988) metamorphic

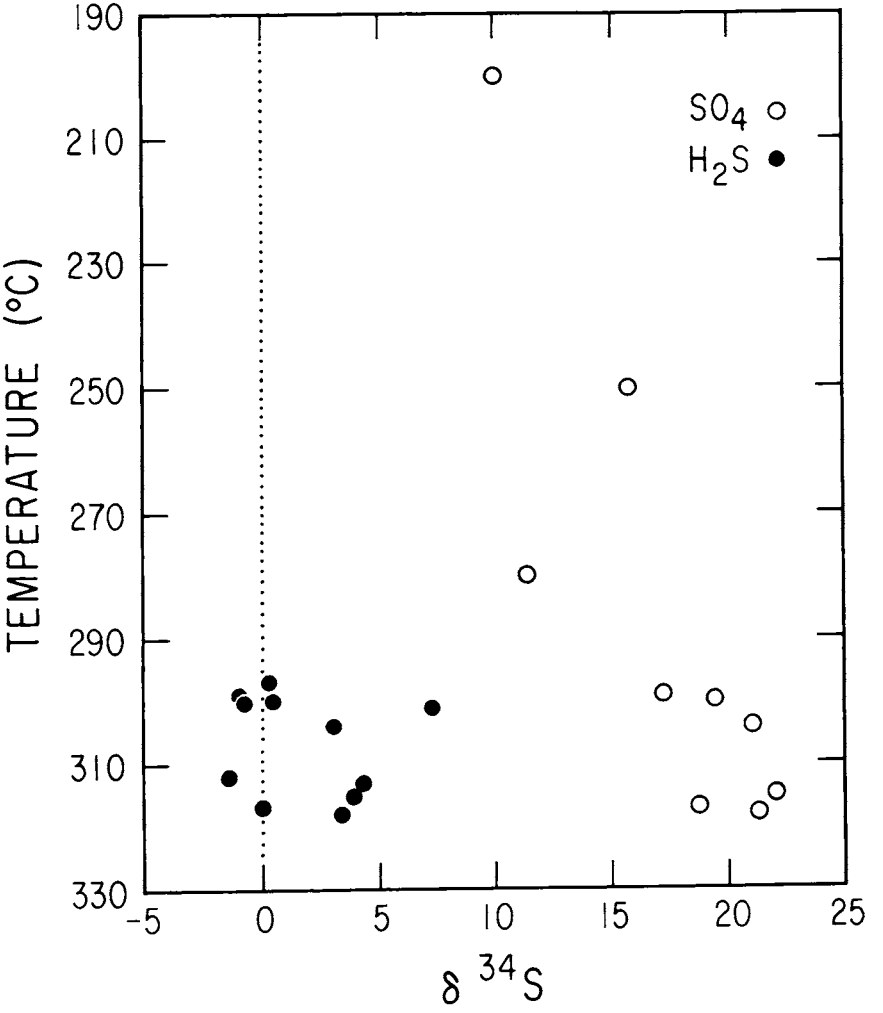

Fig. 11. Plots of conventional sulfur isotope values for aqueous H_2S and SO_4 from geothermal fluids (table 3) versus reservoir temperature (A) and fluid salinity (B).

grade at ≈3 km depth. These data would suggest that the isotopic compositions of stratiform sulfate and sulfide still reflect those of the initial lacustrine depositional environment. Lack of isotopic re-equilibration during metamorphism could be facilitated by the young age of the system, low fluid permeability in the lacustrine shales, low anhydrite solubility in the hypersaline brines, and the isotopic recalcitrance of pyrite at these temperatures noted in several ore deposits (Eldridge and

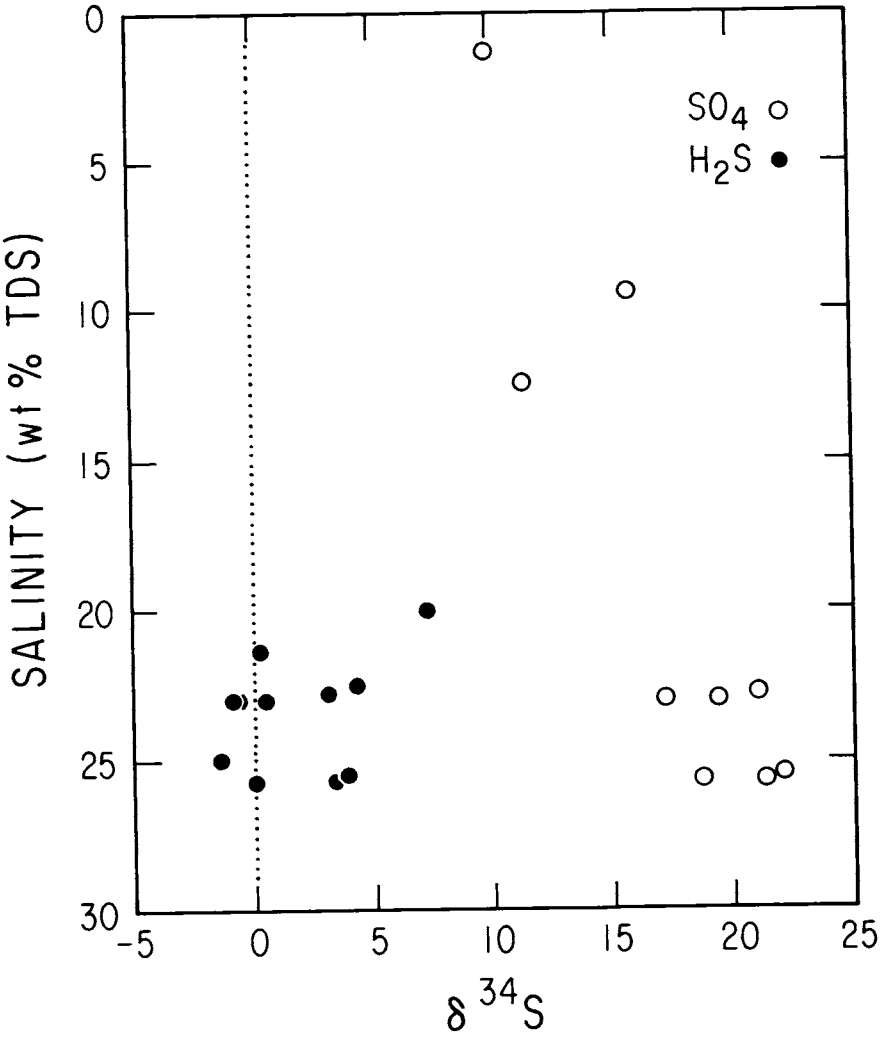

Fig. 11 (continued)

others, 1988b). In contrast, a conventional $\delta^{34}S$ study of the metamorphosed Balmat Pb-Zn deposit by Whelan, Rye, and DeLorraine (1984) revealed that sedimentary pyrite and anhydrite pairs had completely recrystallized and re-equilibrated isotopically at peak metamorphic conditions of 625°C and 6.5 kb. These differences suggest that prolonged amphibolite facies conditions are required for isotopic re-equilibration of sedimentary pyrite-anhydrite intergrowths.

Stratiform Sulfates

The majority of gypsum and anhydrite samples have isotopic compositions (3–20 permil) consistent with those found in lacustrine evaporites precipitated from sulfate derived from continental sources (Holser and Kaplan, 1966). Sulfate input into the Salton Basin has been dominated largely by Colorado River water but punctuated by variable contributions from local streams and storm runoff from the mountain ranges surrounding the Salton Trough, especially at times (like the present) when Colorado River flow was diverted south to the Gulf of California. Unfortunately, we do not know the non-anthropogenic sulfur isotopic composition of modern Colorado River water. While variations in the $\delta^{34}S$ values of anhydrite from different stratigraphic levels (fig. 5) could reflect temporal changes in the sulfur isotopic composition of continental SO_4 carried into the basin, it seems unlikely that such variations in relatively dilute river waters could have profoundly affected the SO_4-rich saline paleo-lakewaters. The $\delta^{34}S$ variations within anhydrites from a given depth interval are as great as those among the different levels, implying that closed-system fractionation effects probably account for most of the isotopic variation in anhydrite. Much of the anhydrite grew as gypsum during shallow sediment diagenesis in a sabkha-type environment (Osborn, ms; Osborn, McKibben, and Williams, 1988). Closed system biogenic reduction of porewater SO_4 during organic matter diagenesis therefore could explain the dramatic zoning in $\delta^{34}S$ revealed by microanalysis of some anhydrites (fig. 6A; S2-14 7708, table 2). The total organic carbon content of the deep SSGS metasediments ranges from 0.06 to 0.47 wt percent, with an average of 0.20 wt percent (C. E. Barker, personal commun. 1988). Although some organics have likely been lost during catagenesis, the total organic content of surface sediments is likewise low, <0.40 wt percent.

Nonetheless, the data in figure 5 suggest that the mean isotopic composition of SO_4 deposited in the Salton Sea basin through time has remained near 10 permil. This is also consistent with the data from the Durmid Hills gypsum (11.6 permil, table 1), which is the unmetamorphosed lateral equivalent of some of the metasediments penetrated in the SSGS (Herzig and Elders, 1988).

The Salton Basin has been isolated from marine waters of the Gulf of California for the past 4 Ma due to progradation of the Colorado River delta westward across the Salton Trough rift (Elders, 1979; Winker and Kidwell, 1986; Winker, ms). Therefore, a Pliocene or younger intrabasinal marine source for any of the lacustrine SO_4 deposited in the host rocks of the SSGS is unlikely. Although extensive Miocene marine gypsum and anhydrite beds occur in the Fish Creek Mountains in the southwest edge of the Salton Trough (Morton, 1977; Ver Planck, 1952; Winker, ms), and runoff and groundwater flow from these mountains presently enters the Salton Basin (Loeltz and others, 1975), the $\delta^{34}S$ values of these marine evaporites (21.1 permil, table 1)

are isotopically too heavy to have been a major source of the ≃10 permil SO_4 deposited in the lacustrine SSGS host rocks.

The anomalously low $\delta^{34}S$ values (≤0 permil) of three of the shallow gypsum samples (table 1; fig. 3) likely resulted from surficial oxidation of biogenic H_2S. The $\delta^{34}S$ value of −30 permil for H_2S from the CO_2 mudpot (table 3) implies that such localized processes may not be uncommon in the young sediments. The ≃0 permil thenardite from the Bertram Mine (table 1) also may have formed from oxidation of H_2S that migrated upward along fault zones. Similar localized surficial processes occurring throughout basin sedimentation may account for some of the variation in $\delta^{34}S$ observed in the SSGS anhydrites.

Stratiform Iron Sulfides

Those stratiform pyrite samples containing isotopically light fine-grained pyrite overgrown by heavier, coarser pyrite (fig. 7A and B; S2-14 6881.5 and 7100.5, table 2) likely record a transition from open-system to closed-system biogenic reduction of SO_4 during burial diagenesis in the deltaic-lacustrine environment. Similar diagenetic overgrowths have been described in pyrite from some marine sediments (Coleman and Raiswell, 1981; Raiswell, 1982; Schmitz, Andersson, and Dahl, 1988). An alternative hypothesis, that the coarse overgrowths are the result of addition of isotopically lighter sulfur during hydrothermal metamorphism, is untenable based on our microanalysis of vein/stratiform sulfide intergrowths. Metasediment samples with a third textural and isotopic generation of pyrtie (fig. 7B; S2-14 7100.5, table 2) illustrate that although hydrothermal fluids have, at times, added new pyrite to the sediments, such pyrite is quite distinct from the sedimentary overgrowth pyrite. These euhedral, isolated hydrothermal pyrite cubes contain tiny inclusions of chalcopyrite that are visible under oil immersion. Additionally, textures in which hydrothermal sulfide completely envelops biogenic sedimentary sulfide (fig. 6D; S2-14 4029, table 2) show no evidence of the formation of pyrite overgrowths by such hydrothermal interactions. The biogenic and hydrothermal sulfur remain distinct and unaffected by one another. Consequently, although a minor fraction of the isotopically heavier disseminated pyrite in sediments (fig. 4) may represent hydrothermally introduced sulfide, we conclude that the isotopically light fine-grained pyrite and coarser overgrowths are all diagenetic in origin, recording a transition to closed-system sulfate reduction during burial.

Sulfides Associated with the Diabase Sill

It is doubtful that the 6 permil total range of $\delta^{34}S$ for pyrite crystals in the diabase sill (fig. 4) is due to the effects of magmatic crystallization (Ohmoto and Rye, 1979). There are no identifiable biogenic sulfides in the metasediment surrounding the diabase, and the pyrite occurrences crosscut and partially replace the diabase (fig. 9) as well as transgress sedimentary layers, so it would appear the sulfides have been introduced

into both rock types. The isotopic composition of this secondary pyrite falls entirely within the range noted for the vein mineralization (fig. 4), suggesting that it was deposited in texturally favorable locations by one and perhaps two (S2-14 9456.6, table 2) later hydrothermal events.

Seawater-basalt interaction experiments indicate that igneous sulfides are easily leached from basalts during water-dominated hydrothermal alteration (Mottl, Holland, and Corr, 1979). Consequently, the lack of evidence for primary igneous sulfide in the altered diabase sill may not mean that igneous sulfide was never present, although the very low water-rock ratios characteristic of alteration in the SSGS (Sturtevant and Williams, 1987) might allow remnants of such sulfide to be preserved. Magnetic and gravity anomalies imply that large gabbroic intrusions occur at depth (Elders, 1979), so shallower diabase sills and dikes could act as channelways for magmatic degassing and sulfur injection into the metasediments.

The surface rhyolite domes contain xenoliths of diabase (Robinson, Elders, and Muffler, 1976; C. T. Herzig, in preparation), implying that their eruption post-dates the intrusion of the diabase sill. Because the thermal structure of the SSGS appears to be linked intimately with the arc of rhyolite domes (fig. 2), it is logical to conclude that they and their deep-seated source magma are the most likely potential sources of juvenile sulfur in the SGGS. However, as noted above, examination of the rhyolites has not yet revealed any primary igneous sulfides.

Although we cannot completely rule out a contribution of sulfur from magmatic sources, the fluid sulfur isotopic data discussed below coupled with the abundance of evaporitic anhydrite in the host metasediments indicate that hydrothermal SO_4 reduction is the main source of H_2S in the SSGS brines.

Vein Minerals, Aqueous H_2S and SO_4

The SHRIMP $\delta^{34}S$ data for vein sulfides show a wider distribution than the conventional data (figs. 3 and 4), but this probably reflects the much greater number of microanalyses. Both data sets show an $\simeq 0$ permil mean.

Isotopic zoning within some veins (fig. 7C; S2-14 2999.5, table 2), isotopic variability among H_2S samples from different wells and from different flow-tests of the same well (table 3), and apparent isotopic disequilibrium between ejecta pyrite and fluid H_2S from the 1898 m (6227 ft) flow-zone in the well S2-14 illustrate that the isotopic composition of fluid H_2S has varied in time and space. It seems likely that many of these variations were caused by closed-system isotopic fractionation effects during precipitation of metals from fluids that are low in total sulfur (Ohmoto, 1986). Additional variations could be caused by inhomogeneities in the source of sulfide (see below) or by changes in the redox state of the brines, as well as by periodic injections of isotopically distinct sulfur from a magmatic source.

The greatest shift in isotopic composition of aqueous H_2S apparently took place during formation of the anomalous type 1 vein (−22 permil; fig. 7D). This isotopic change occurred with no change in vein mineralogy compared with other type 1 veins, but the anomalous vein occurs in an abnormally thick shale sequence. It seems likely that the isotopic composition of sulfides in this vein was influenced by H_2S derived from organic matter. McKibben and others (1987) and McKibben, Andes, and Williams (1988) have proposed that the type 1 veins formed early in the history of the SSGS, during heating and expulsion of connate fluids. Therefore, catagenesis and release of isotopically light H_2S from organic matter in shales during this early heating stage is feasible.

No unequivocal examples of vein sulfate mineralization have been found. The sulfates that might be interpreted as vein material in drill cuttings (table 1) often occur in drillcore as cement in brecciated shale having isotopic compositions similar to stratiform sulfate (MM-11 3422.8, table 2). Such "vein" anhydrites may represent locally dissolved and reprecipitated evaporitic material rather than hydrothermally introduced sulfate (McKibben, Williams, and Okubo, 1988), making it difficult to use these data to constrain the isotopic composition of the aqueous sulfate. The direct measurements of the sulfur isotopic composition of fluid SO_4 show that there is considerable variation between shallow fluids and deep brines. As will be discussed below, this likely reflects hydrothermal redox processes affecting SO_4 in the deep brines.

Fluid Sulfate-Sulfide Isotopic Equilibrium

The observed sulfur isotopic fractionation between coexisting aqueous H_2S and SO_4 in the deep hypersaline brines (18–19 permil at 300°–320°C, table 3) agrees very well with the experimentally determined equilibrium fractionation (19–20 permil, Ohmoto and Lasaga, 1982; Sakai and Dickson, 1978) for dilute solutions. Therefore, the equilibrium sulfur isotopic fractionation between H_2S and SO_4 is not affected by the very high salinities of these brines at these temperatures. This observation is very encouraging to those studying and interpreting sulfur isotopic variations in ore deposits that formed from saline hydrothermal fluids! It is not surprising that equilibrium has been attained: residence times for brines in the SSGS appear to be relatively long at 10^2 to 10^3 yrs (Zukin and others, 1987), whereas at Salton Sea reservoir brine pH conditions (pH = 5.4, McKibben and Elders, 1985) only 140 days would be required to establish equilibrium at 300°C (Ohmoto and Lasaga, 1982; Sakai and Dickson, 1978).

Sources of Aqueous Sulfate and Sulfide

The similarity between the mean $\delta^{34}S$ values of SO_4 in the low-salinity SSGS geothermal fluids (table 3, fig. 11B) and sedimentary gypsum and anhydrite in the host-rocks ($\simeq$10 permil) is consistent with the notion that SO_4 in these shallow fluids is derived directly from

dissolution of these sedimentary sulfates. It does not seem possible that some of the shallow aqueous SO_4 could be generated by oxidation of H_2S in the deep hypersaline brines at the fluid interface, because quantitative oxidation would produce SO_4 that is isotopically light ($\simeq$0 permil), and the acidity generated by such oxidation does not seem consistent with the abundance of carbonates in the veins and shallow sediments (McDowell and Paces, 1985). Also, the concentration of SO_4 in the shallow fluids typically exceeds that of H_2S in the hypersaline brines. There clearly exists a need for more analyses of the isotopic composition of SO_4 in the shallow low-salinity fluids, but unfortunately these fluids are not economic for power generation, and geothermal wells are therefore rarely completed and flowed at these shallow depths.

The $\simeq$10 permil S^{34} enrichment of SO_4 in the deep hypersaline brines ($\simeq$20 permil) relative to the mean composition of deep host rock anhydrite ($\simeq$10 permil) indicates that simple dissolution of host-rock anhydrite is not the sole process influencing the isotopic composition of aqueous SO_4 in the deep brines. Contributions of isotopically heavy SO_4 from buried marine sediments correlative with the Fish Creek Mountains evaporites (21.1 permil, table 1) or deep fossil connate seawater could be a source of heavy SO_4, but they are unlikely to have been major factors. The Miocene evaporites occur only at the margins of the Salton Trough where they formed early in the history of rift development, so their buried equivalents cannot exist at depth in the young central part of the active Salton Trough rift. Finally, the H and O isotopic compositions of the water in the hypersaline brines simply rule out a marine precursor or component for these fluids (Craig, 1966, 1969; McKibben and others, 1987; Williams and McKibben, 1989).

Because no sources of isotopically heavy SO_4 are known in or near the SSGS, the consistent ^{34}S enrichment of aqueous SO_4 in the deep hypersaline brines *must* be caused by high temperature reduction of SO_4 dissolved from the host rock anhydrite in the deeper parts of the hydrothermal system. Given the demonstrated isotopic equilibrium between aqueous H_2S and SO_4 in the deep brines and direct measurements of the brine chemistry and temperature (table 3), this hypothesis can be evaluated using the total fluid sulfur isotopic mass balance equation of Ohmoto (1986):

$$\delta^{34}S_{\Sigma S} = \delta^{34}S_{H_2S} + \Delta_{SO_4-H_2S}(R/(1 + R))$$

where R is the mole ratio of sulfate and sulfide in solution. Two approaches can be taken to applying the mass balance equation to the SSGS brines: (1) calculating $\delta^{34}S_{\Sigma S}$ for individual pairs of H_2S and SO_4 analyses where the mole ratios are known, and (2) calculating a mean $\delta^{34}S_{\Sigma S}$ from the mean mole ratio and isotopic values for all fluid analyses.

Of the six pairs of H_2S and SO_4 $\delta^{34}S$ analyses given in table 3, the molal ratio R is known for only two (S2-14-1 and DR-3) because of the above-mentioned recovery problems caused by use of $ZnCl_2$ rather than

$CdCl_2$ solutions to strip H_2S from some of the steam phase samples. Using the data in table 3, we obtain values of $\delta^{34}S_{\Sigma S}$ equal to 14.9 permil for S2-14-1 and 11.1 permil for DR-3. These values agree well with the mean isotopic composition of deep host rock anhydrites (fig. 4).

Taking the more general approach, the mean value of $\delta^{34}S$ for brine H_2S is 1.8 permil, the mean $\Delta_{SO_4-H_2S}$ value is 18.4 permil, and the mean value of R in the brines is 1.16 (table 3). These values yield a mean $\delta^{34}S_{\Sigma S}$ value equal to 11.7 permil, a value that agrees very well with the mean isotopic composition of deep host rock anhydrites (fig. 4). Consequently, both approaches to the mass balance calculation support the hypothesis that brine H_2S is derived mainly by hydrothermal reduction of SO_4 derived from dissolution of anhydrite in the reservoir rocks. An equilibrium 50 percent reduction of anhydrite-derived SO_4 ($\simeq$10 permil initially) would yield equimolal amounts of S^{34}-depleted H_2S ($\simeq$0 permil) and S^{34}-enriched SO_4 ($\simeq$20 permil) in the deep hypersaline brines at $\simeq$300°C.

The deep hypersaline reservoir brines are rich in Fe and Mn (1000–2000 ppm each) and have high Fe/Zn + Pb and H_2S/SO_4 ratios relative to the overlying less saline fluids, implying that these deep brines have a relatively reduced oxidation state (McKibben and others, 1987; Williams and McKibben, 1989). Therefore, interaction of these hot, upwelling brines with the large reservoir of evaporitic SO_4 in the host sediments could promote reduction and H_2S generation. Partial replacement of sedimentary anhydrite by epidote and other metamorphic phases has been observed in the SSGS at depths greater than 1.3 km (Cho, Liou, and Bird, 1988; Osborn, McKibben, and Williams, 1988; Osborn and McKibben, in preparation), implying that reactions of the type:

$$2CaSO_4 + 8Fe^{2+} + 3H_4SiO_4 + 4.5H_2O = Ca_2Fe_3Si_3O_{12}OH + 2.5Fe_2O_3 + 18H^+ + SO_4^{2-} + H_2S$$

may be responsible for hydrothermal SO_4 reduction and H_2S generation. Such a reaction is consistent with the epidote-hematite paragenesis of type 2 veins (McKibben, Andes, and Williams, 1988) and may effectively buffer the concentrations of aqueous sulfur species in the SSGS brines. The coincidence of the temperatures of isotopic equilibrium between H_2S and SO_4 (table 3) and the temperatures at which anhydrite replacement reactions occur support this hypothesis.

The mass balance calculation shows that the *mean* isotopic composition of H_2S in the deep brines ($\simeq$2 permil, table 3) can be accounted for by this hydrothermal reduction model, but the large range of individual values for both brine H_2S (fig. 3) and vein sulfides (fig. 4) must reflect variations in the original $\delta^{34}S$ values of the source anhydrite as well as the local or episodic influence of secondary effects on isotopic fractionation. Possible secondary factors include magmatic sulfur input, variable dissolution of biogenic pyrite contained within anhydrite, and closed-system fractionation effects during vein sulfide precipitation.

The role of magmatic input seems minor; data from this study have shown that the shallow diabase sill in S2-14 contains no primary igneous sulfides (or their leached remnants) and has been hydrothermally altered and veined by later sulfide-depositing hydrothermal fluids. Additionally, the surface rhyolite domes contain no evidence of primary igneous sulfide; however, their intrusive equivalents have not yet been penetrated by drilling. It is possible that sulfur degassing of deeper intrusions occurs later than dike intrusion and dome extrusion, so that periodic magmatic contributions to brine H_2S occur. Unfortunately, evaluation of a possible magmatic sulfur component in the brines and veins must await deeper drilling in the SSGS.

Magmatic assimilation and homogenization of metasediments could produce a magmatic fluid with H_2S near 0 permil, if such a process caused quantitative reduction of SO_4 contained in sedimentary sulfate and if the sediments contained a 1:1 molar ratio of sedimentary sulfide to sulfate. However, sedimentary sulfate is far more abundant than sedimentary sulfide in the SSGS host-rocks.

Fluctuations in the isotopic composition of the aqueous H_2S deposited in vein sulfides also could have been generated by dissolution of biogenic sulfides in the host sediments. It has already been shown that variation in the isotopic composition of H_2S at the site of vein deposition cannot be due to contamination by dissolution of stratiform pyrite, because microanalysis of samples with intergrown vein and sedimentary sulfides shows no influence of the diagenetic sulfur component on the isotopic composition of hydrothermal sulfides. However, it is possible that at higher temperatures (greater depth) some stratiform pyrite is dissolved along with the source anhydrite. Partial reduction of the anhydrite's sulfate along with dissolution of some intergrown diagenetic sulfide could result in a fluid with $\delta^{34}S$ values less than 0 permil.

Fluid H_2S isotopic compositions could also be made either more positive or negative during vein sulfide precipitation if the fluid contained more metals than sulfur. Precipitation of sulfides could then significantly reduce the H_2S content of the fluid, making it isotopically lighter if pyrite were precipitated or isotopically heavier if galena were precipitated (Ohmoto, 1986). Local reduction of aqueous sulfate at the site of deposition could also produce isotopically heavy H_2S and cause aqueous H_2S/vein mineral disequilibrium as noted in the S2-14 flow-zone samples and in ocean floor hydrothermal chimneys (Shanks and Seyfried, 1987).

The fluid forming the earliest type 1 mineralization with the anomalously light isotopic composition (−22 permil, S2-14 8134.5, table 2) must have had a different sulfur source. McKibben, Andes, and Williams (1988) conclude that this early vein mineralization may have formed during heating and expulsion of reduced connate fluids, possibly deriving reduced sulfur from fluids that leached isotopically light H_2S from biogenic sulfides in sediments or through catagenesis of detrital organic matter. However, our microbeam analysis of textures suggests

that the first process is not feasible. An organic sulfur influence is more likely, although both surface sediments and deep shales in the SSGS contain relatively low amounts of total organic carbon (generally less than 0.5 wt percent with an average of 0.2 wt percent; C. E. Barker, personal commun., 1988).

In summary, the mean isotopic composition of H_2S in the brines and vein sulfides can be accounted for by a model involving equilibrium hydrothermal reduction of SO_4 derived from host-rock anhydrite at $\simeq 300\,^{\circ}C$. $\delta^{34}S$ variations of ± 10 permil are caused by variations in source anhydrite compositions and by various secondary processes that are local or episodic in nature. These include variable co-dissolution of biogenic pyrite contained in source anhydrite, sulfide precipitation-induced isotopic fractionation at the site of deposition, and episodic input of juvenile magmatic sulfur. No direct evidence of a major magmatic sulfur input has been found, but unequivocal evaluation of the role of such a source will require deeper drilling in the SSGS.

Vein Mineral Precipitation Mechanisms

Sulfide vein mineralization occurs sporadically throughout the 3 km drilled depth of the SSGS, but is is most concentrated at depths of 610 to 1524 m (2000–5000 ft). This coincides with the depth interval occupied by the interface between hypersaline brines and overlying lower-salinity fluids (McKibben, Andes, and Williams, 1988; Williams, 1988; Williams and McKibben, 1989). Coincidence of the brine interface and abundance of vein mineralization suggest that the main mechanism involved in ore precipitation is cooling and dilution of the upwelling H_2S- and metal-bearing brines during mixing with the shallow fluids (McKibben, Andes, and Williams, 1988). H_2S, derived chiefly from hydrothermal reduction of sedimentary anhydrite at depth, is transported upward in the hot brines and is precipitated as sulfides during the mixing process at the fluid interface.

Precipitation of some sulfides requires partial oxidation of H_2S to sulfanes (S_2^{2-} in pyrite, S_2^{3-} in chalcopyrite). This may occur during fluid mixing at the interface and could also account for some of the $\delta^{34}S$ variations of the vein sulfides.

CONCLUSIONS AND IMPLICATIONS FOR SULFUR ISOTOPE GEOCHEMISTRY AND ORE GENESIS

Combined ore microscopic, conventional, and ion microprobe isotopic data have been used to elucidate the processes involved in and sources of sulfur for the sediment-hosted vein mineralization in the SSGS. These data indicate that, regardless of the low sulfur content of the brines, it is aqueous H_2S that is used in precipitating the ore minerals and not sulfur derived locally from the replacement of biogenic sulfide. Biogenic sulfide may become indirectly involved as a minor contributor of reduced sulfur to the hydrothermal fluid at depth in the hydrothermal system, but the major component of aqueous H_2S comes from

reduction of sulfate derived from dissolution of abundant non-marine metaevaporitic anhydrite in the host metasediments. Igneous rocks, sampled from a diabase sill cored at 3 km depth, are altered and veined with hydrothermal sulfide and do not seem to have been a source of sulfur. Contrary to initial impressions from earlier reconnaissance conventional isotopic studies, there are many generations of vein sulfides embracing a total range in sulfur isotopic composition exceeding 30 permil. While the majority of vein sulfide $\delta^{34}S$ values cluster around 0 permil, substantial variations in isotopic composition are evident. They may result from several processes, including partial oxidation of H_2S in the hypersaline brines during the fluid mixing that leads to vein sulfide precipitation (McKibben, Andes, and Williams, 1988), fractionation accompanying sulfide precipitation in fluids with low sulfur contents (Ohmoto, 1986), natural variability in the isotopic composition of evaporitic sulfate minerals tapped as the sulfur source, or minor dissolution of biogenic sulfide held in and dissolved with the anhydrite.

Moreover, potential shortfalls in application of only one of these three investigative methods to complex natural systems have been highlighted. Microscopic variations in $\delta^{34}S$ values within and among minerals, like those shown in figures 6 and 7, have very significant implications for conventional sampling practices in sulfur isotope geochemistry. Typically, milligram levels of sulfate or sulfide samples are used, and great care is taken to prepare pure mineral separates by physical and/or chemical techniques. It is clear from examples in this study that such attempts may actually bias the analytical results, because composite grains would likely be rejected as impure, and it is often the case that considerable isotopic variation can be found adjacent to grain boundaries, while large areas of a single phase may be isotopically homogeneous (fig. 6A). Similar circumstances may arise with central portions of veins being of one isotopic composition and the margins of another (fig. 7C). Small portions of the vein mineral margins, which might cling to wall rock and be overlooked for conventional analysis, might hold important information regarding sulfide precipitation. For such material, selective dissolution might be advisable; however, it would necessarily average the isotopic compositions of all generations of a given phase being dissolved. In samples like the stratiform sulfides (fig. 7A and B), only an average $\delta^{34}S$ value would be found through dissolution techniques, masking important information concerning the changing diagenetic environment and later incursions of hydrothermal fluids into the sediment.

Examination of ore/diagenetic mineral textural relations naturally plays a crucial role in formulating theories of sediment-hosted ore deposit genesis and understanding metamorphic effects on sediments. It has often been suggested, for example, that ore minerals may precipitate when metal-rich, sulfur-poor fluids encounter sediments rich in diagenetic sulfides. However, close optical and microbeam isotopic inspection

of SSGS samples has shown that, although vein sulfides may enclose diagenetic sulfides, there has been no local replacement and recycling of sedimentary sulfide. Textural proximity alone cannot be used to substantiate chemical and isotopic communication. Conversely, close proximity does not always indicate closed isotopic systems as has sometimes been interpreted for apparent metamorphic recrystallization of fine-grained, poorly organized, diagenetic sulfides to coarse-grained and euhedral crystals. As shown in this study, spatially overlapping morphologies can represent distinct non-metamorphic (diagenetic) crystal growth events, and fine-grained pyrite can retain its morphological characteristics to at least lower amphibolite facies metamorphic conditions.

Our studies illustrate the tremendous potential insights available through combination of ore textural studies with the powerful new technique of *in situ* isotopic microanalysis. When combined with conventional isotopic analyses of fluid species, studies in active geothermal systems can place critical constraints on petrogenetic and ore-forming processes.

ACKNOWLEDGMENTS

This research was supported by NSF grant EAR-8617430 (M.A.M) and in part by DOE grant DE-FG03-85ER13408 (M.A.M). Financial support for C.S.E. was provided by the Australian Research Grants Scheme; the visiting fellowship granted by the Research School of Earth Sciences is also acknowledged. M.A.M. is especially grateful to A. E. Williams for discussions on fluid chemistry and for patiently teaching the art of geothermal well sampling. J. P. Andes Jr., W. L. Osborn, and J. L. Mehegan aided in sample selection and preparation. Magma Power Co., Dow Chemical USA, and Kennecott Corp. provided access to commerical well samples. P. W. Kasameyer and T.-C. Lee allowed access to samples from LBL shallow thermal gradient wells. D. E. White generously provided additional details on his 1968 $\delta^{34}S$ data. We thank R. O. Rye for providing conventional $\delta^{34}S$ analyses. We also thank C. W. Field of Oregon State University for contributing anhydrite for our use as an analytical standard. His conventional analysis and that of R. A. Both, University of Adelaide, are also appreciated. Finally, we thank W. A. Elders for spawning the unique opportunities provided by the Salton Sea Scientific Drilling Project. The manuscript was improved by the comments of R. O. Rye, W. C. Shanks, III, and an anonymous third journal reviewer.

REFERENCES

Arnold, M., and Partida, E. G., 1987, Le systeme hydrothermal actuel de Los Humeros (Mexique): Etat du systeme SO_4^{2-}-H_2S a 300°C, origine du soufre et phenomenes d'oxydation associes a l'ebullition du fluide ascendant; Minealium Deposita, v. 22, p. 90–98.

Babcock, E. A., 1974, Geology of the northeast margin of the Salton Trough, Salton Sea, California: Geological Society of America Bulletin, v. 85, p. 321–332.

Brown, P. R. L., and Elders, W. A., 1976, Hydrothermal alteration of diabase, Heber geothermal field, Imperial Valley, California [abs.]: Geological Society of America, Abstracts with Program, v. 8, p.793.

Browne, P. R. L., Rafter, T. A., and Robinson, B. W., 1975, Sulfur isotopic variations in nature, 11. Sulfur isotope ratios of sulfides from the Broadlands geothermal field, New Zealand: New Zealand Journal of Science, v. 18, p. 35–40.

Charles, R. W., Janecky, D. R., Goff, F., and McKibben, M. A., 1988, Chemographic and thermodynamic analysis of the paragenesis of the major phases in the vicinity of the 6120 ft (1866 m) flow-zone, California State 2-14: Journal of Geophysical Research, v. 93, p. 13145–13158.

Cho, M., Liou, J. G., and Bird, D. K., 1988, Prograde phase relations in the California State 2-14 well meta-sandstones, Salton Sea geothermal field: Journal of Geophysical Research, v. 93, p. 13081-13103.

Coleman, M. L., and Raiswell, R., 1981, Carbon, oxygen and sulfur isotope variations in concretions from the Upper Lias of N. E. England: Geochimica et Cosmochimica Acta, v. 45, p. 329–340.

Craig, H., 1966, Isotopic composition and origin of the Red Sea and Salton Sea geothermal brines: Science, v. 154, p. 1544–1548.

———— 1969, Discussion: Source fluids for the Salton Sea geothermal system: American Journal of Science, v. 267, p. 249–255.

Elders, W. A., 1979, The geological background of the geothermal fields of the Salton Trough: *in* Elders, W. A., ed., Geology and Geothermics of the Salton Trough: University of California, Riverside, California, Campus museum contribution no. 5, p. 1–19.

———— 1987, Igneous rocks in the SSSDP well and in the Salton Trough [abs.]: EOS Transactions of the American Geophysical Union, v. 68, p. 446.

Elders, W. A., Rex, R. W., Meidav, T., Robinson, P. T., and Biehler, S., 1972, Crustal spreading in southern California: Science, v. 178, p. 15–24.

Elders, W. A., and Sass, J. H., 1988, The Salton Sea scientific drilling project: its scientific significance: Journal of Geophysical Research, v. 93, p. 12953–12968.

Eldridge, C. S., Barton, P. B., Jr., and Ohmoto, H., 1983, Mineral textures and their bearing on formation of the Kuroko orebodies, *in* Ohmoto, H., and Skinner, B. J., eds., The Kuroko and Related Volcanogenic Massive Sulfide Deposits: Economic Geology Monograph 5, p. 241–281.

Eldridge, C. S., Compston, W., Williams, I. S., Both R. A., Walshe, J. L., and Ohmoto, H., 1988a, Sulfur isotope variability in sediment-hosted massive sulfide deposits as determined using the ion microprobe SHRIMP: I. An example from the Rammelsberg orebody: Economic Geology, v. 83, p. 205–211.

Eldridge, C. S., Compston, W., Williams, I. S., Patterson, D. J., Walshe, J. L., and Both, R. A., 1985, Ion microprobe determination of sulfur isotopic compositions of sulfides from the Mt. Isa Pb/Zn orebody [abs.]: Geological Society of America, Abstracts with Program, v. 17, p. 573.

Eldridge, C. S., Compston, W., Williams, I. S., and Walshe, J. L., 1988b, Sulfur isotope analyses on the SHRIMP ion microprobe: *in*Shanks, W. C., III, and Criss, R. E., eds., New Frontiers in Stable Isotope Research: Laser probes, ion probes, and small sample analysis, U. S. Geological Survey Bulletin, in press.

Eldridge, C. S., Compston, W., Williams, I. S., Walshe, J. L., and Both, R. A., 1987, In situ microanalysis for $^{34}S/^{32}S$ ratios using the ion microprobe SHRIMP: International Journal of Mass Spectrometry and Ion Processes, v. 76, p. 65–83.

Eldridge, C. S., Williams, N., Compston, W., and Walshe, J. L., 1988c, SHRIMP ion microprobe investigation of the sulfur isotopic composition of the H. Y. C. Pb-Zn deposit, McArthur River, Australia [abs.]: Geological Society of America, Abstracts with Programs, v. 20, no. 7, p. 303.

Gilluly, J., 1946, The Ajo mining district, Arizona: U. S. Geological Survey Professional Paper 209, 112 p.

Helgeson, H. C., 1968, Geologic and thermodynamic characteristics of the Salton Sea geothermal system: American Journal of Science, v. 266, p. 129–166.

Herzig, C. T., and Elders, W. A., 1988, Igneous rocks in the State 2-14 research borehole, Salton Sea scientific drilling project, California, U.S.A.: Journal of Geophysical Research, v. 93, p. 13069–13080.

Herzig, C. T., Mehegan, J. M., and Stelting, C. E., 1988, Lithostratigraphy of an active pull-apart basin: Salton Sea Scientific Drilling Project: Journal of Geophysical Research, v. 93, p. 12969–12980.

Holser, W. T., and Kaplan, I. R., 1966, Isotope geochemistry of sedimentary sulfates: Chemical Geology, v. 1, p. 93–135.

Johnson, C. E., and Hadley, D. M., 1976, Tectonic implications of the Brawley earthquake swarm, Imperial Valley, California, January 1975: Bulletin of the Seismological Society of America, v. 66, 1133–1144.

Kusakabe, M., 1974, Sulfur isotopic variations in nature 10. Oxygen and sulfur isotope study of Wairakei geothermal well discharges: New Zealand Journal of Science, v. 17, p. 183–191.

Loeltz, O. J., Ireland, B., Robison, J. H., and Olmsted, F. H., 1975, Geohydrologic reconnaissance of the Imperial Valley, California: U.S. Geological Survey Professional Paper 486-K, 54 p.

McDowell, S. D., and Elders, W. A., 1980, Authigenic layer silicate minerals in borehole Elmore 1, Salton Sea geothermal field, California, U.S.A: Contributions to Mineralogy and Petrology, v. 74, p. 293–310.

———— 1983, Allogenic layer silicate minerals in borehole Elmore #1, Salton Sea geothermal field, California: American Mineralogist, v. 68, p. 1146–1159.

McDowell, S. D., and Paces, J. B., 1985, Carbonate alteration minerals in the Salton Sea geothermal system, California, U.S.A.: Mineralogical Magazine, v. 49, p. 469–479.

McKibben, M. A., Andes, J. P. Jr., and Williams, A. E., 1988, Active ore-formation at a brine interface in metamorphosed deltaic-lacustrine sediments: the Salton Sea geothermal system, California: Economic Geology, v. 83, p. 511–523.

McKibben, M. A., and Elders, W. A., 1985, Fe-Zn-Cu-Pb mineralization in the Salton Sea geothermal system, Imperial Valley, California: Economic Geology, v. 80, p. 539–559.

McKibben, M. A., Williams, A. E., Elders, W. A., and Eldridge, C. S., 1987, Saline brines and metallogenesis in a sediment-filled rift: the Salton Sea geothermal system, California: Applied Geochemistry, v. 2., p. 563–578.

McKibben, M. A., Williams, A. E., and Okubo, S., 1988, Metamorphosed Plio-Pleistocene evaporites and the origins of hypersaline brines in the Salton Sea geothermal system, California: fluid inclusion evidence: Geochimica et Cosmochimica Acta, v. 52., p. 1047–1056.

Morton, P. K., 1977, Geology and mineral resources of Imperial County, California: California Division of Mines and Geology, County Report no. 7, 104 pp.

Mottl, M. J., Holland, H. D., and Corr, R. F., 1979, Chemical exchange during hydrothermal alteration of basalt by seawater-II. Experimental results for Fe, Mn and sulfur species: Geochimica et Cosmochimica Acta, v. 43, p. 869–884.

Muffler, L. J. P., and White, D. E., 1968, Origin of CO_2 in the Salton Sea geothermal system, southeastern California, U.S.A.: International Geological Congress, 23d, Prague, Proc., v. 17, p. 185–194.

———— 1969, Active metamorphism of upper Cenozoic sediments in the Salton Sea geothermal field and the Salton trough, southeastern California: Geological Society of America Bulletin, v. 80, p. 157–182.

Newmark, R. L., Kasameyer, P. W., and Younker, L. W., 1988, Shallow drilling in the Salton Sea region: the thermal anomaly: Journal of Geophysical Research, v. 93, p. 13005–13024.

Newmark, R. L., Kasameyer, P. W., Younker, L. W., and Lysne, P. C., 1986, Research drilling at the Salton Sea geothermal field, California: the shallow thermal gradient project: EOS Transactions of the American Geophysical Union, v. 67, p. 698–707.

Ohmoto, H., 1986, Stable isotope geochemistry of ore deposits, *in* Valley, J. W., Taylor, H. P., Jr., and O'Neil, J., Eds., 1986, Stable Isotopes in High Temperature Geological Processes: Mineralogical Society of America, Reviews in Mineralogy, v. 16, p. 491–560.

Ohmoto, H., and Lasaga, A. C., 1982, Kinetics of reactions between aqueous sulfates and sulfides in hydrothermal systems: Geochimica et Cosmochimica Acta, v. 46, p. 1727–1746.

Ohmoto, H., and Rye, R. O., 1979, Isotopes of Sulfur and Carbon, *in* Barnes, H. L., Ed., Geochemistry of Hydrothermal Ore Deposits: New York, Wiley-Interscience, p. 509–567.

Osborn, W. L., ms, 1988, Formation, diagenesis and metamorphism of sulfate minerals in the Salton Sea geothermal system, California: M.S. thesis, University of California, Riverside, 150 p.

Osborn, W. L., McKibben, M. A., and Williams, A. E., 1988, Formation, diagenesis and metamorphism of lacustrine sulfates under high geothermal gradients in an active continental rift zone: Geological Society of America, Abstracts with Program, v. 20, no. 7, p. 51.

Raiswell, R., 1982, Pyrite texture, isotopic composition and the availability of iron: American Journal of Science, v. 282, p. 1244–1263.

Robinson, P. T., Elders, W. A., and Muffler, L. J. P., 1976, Quaternary volcanism in the Salton Sea geothermal field, Imperial Valley: Geological Society of America Bulletin, v. 87, p. 347–360.

Rye, R. O., and Ohmoto, H., 1974, Sulfur and carbon isotopes and ore genesis: a review: Economic Geology, v. 69, p. 826–842.

Sakai, H., and Dickson, F. W., 1978, Experimental determination of the rate and equilibrium fractionation factors of sulfur isotope exchange between sulfate and sulfide in slightly acid solutions at 300°C and 1000 bars: Earth and Planetary Science Letters, v. 39, p. 151–161.

Sasaki, A., Arikawa, Y., and Folinsbee, R. E., 1979, Kiba reagent method of sulfur extraction applied to isotopic work: Bulletin of the Geological Survey of Japan, v. 30, p. 241–245.

Sass, J. H., Priest, S. S., Duda, L. E., Carson, C. C., Hendricks, J. D., and Robison, L. C., 1988, Thermal regime of the State 2-14 well, Salton Sea Scientific Drilling Project: Journal of Geophysical Research, v. 93, p. 12995–13004.

Schmitz, B., Andersson, P., and Dahl, J., 1988, Iridium, sulfur isotopes and rare earth elements in the Creataceous-Tertiary boundary clay at Stevns Klint, Denmark: Geochimica et Cosmochimica Acta, v. 52, p. 229–236.

Schoen, R., and Rye, R. O., 1970, Sulfur isotope distribution in solfataras, Yellowstone National Park: Science, v. 170, p. 1082–1084.

Shanks, W. C., III, and Seyfried, W. E., Jr., 1987, Stable isotope studies of vent fluids and chimney minerals, southern Juan de Fuca Ridge: sodium metasomatism and seawater sulfate reduciton: Journal of Geophysical Research, v. 92, p. 11387–11399.

Shearer, C. K., Papike, J. J., Simon, S. B., Davis, B. L., Rick, F. J., and Laul, J. C., 1988, Mineral reactions in altered sediments from the California State 2-14 well: variations in the modal mineralogy, mineral chemistry and bulk composition of the SSSDP core: Journal of Geophysical Research, v. 93, p. 13104–13122.

Skinner, B. J., White, D. E., Rose, H. J., Jr., and Mays, R. E., 1967, Sulfides associated with the Salton Sea geothermal brine: Economic Geology, v. 62, p. 316–330.

Steiner, A., and Rafter, T. A., 1966, Sulfur isotopes in pyrite, pyrrhotite, alunite and anhydrite from steam wells in the Taupo volcanic zone, New Zealand: Economic Geology, v. 61, p. 1115–1129.

Sturtevant, R. G., and Williams, A. E., 1987, Oxygen isotopic profiles of the State 2-14 geothermal well: evidence for a complex history: EOS Transactions of the American Geophysical Union, v. 68, p. 445.

Taylor, B. E., 1986, Magmatic volatiles: isotopic variation of C, H and S: in Valley, J. W., Taylor, H. P., Jr., and O'Neil, J., eds., 1986, Stable Isotopes in High Temperature Geological Processes: Mineralogical Society of America, Reviews in Mineralogy, v. 16, p. 185–226.

———— 1987, Stable isotope geochemistry of ore-forming fluids, *in* Kyser, T. K., Ed., Short Course in Stable Isotope Geochemistry of Low Temperature Fluids: Mineralogical Association of Canada, v. 13, p. 337–445.

Thode, H. G., Monster, J., and Dunford, H. B., 1961, Sulfur isotope geochemistry: Geochimica et Cosmochimica Acta, v. 25, p. 159–174.

Torssander, P., 1986, Origin of sulfur in Icelandic geothermal fluids: International Symposium on Water-Rock Interaction, 5th, Reykjavik, Orkustofnun, p. 583–586.

Truesdell, A. H., Rye, R. O., Whelan, J. F., and Thompson, J. M., 1978, Sulfate chemical and isotopic patterns in thermal waters of Yellowstone Park, Wyoming, *in* Zartman, R. E., ed., Short Papers, 4th International Conference on Geochronology, Cosmochronology, and Isotope Geology: U.S. Geological Survey Open-File Report, no. 78-701, p. 435–436.

Ver Planck, W. E., 1952, Gypsum in California: California Division of Mines Bulletin 163, p. 27–35.

Whelan, J. F., Rye, R. O., and DeLorraine, W., 1984, The Balmat-Edwards zinc-lead deposits-synsedimentary ore from Mississippi Valley-type fluids: Economic Geology, v. 79, p. 239–265.

White, D. E., 1968, Environments of generation of some base-metal ore deposits: Economic Geology, v. 63, p. 301–335.

White, D. E., Anderson,E. T., and Grubbs, D. K., 1963, Geothermal brine well: Mile-deep drill hole may tap ore-bearing magmatic water and rocks undergoing metamorphism: Science, v. 139, p. 919–922.

Williams, A. E., 1988, Delineation of a brine interface in the Salton Sea geothermal system, California: Geothermal Resources Council, Transactions, v. 12, p. 151–157.

Williams, A. E., and McKibben, M. A., 1989, A brine interface in the Salton Sea geothermal system, California: fluid geochemical and isotopic characteristics: Geochimica et Cosmochimica Acta, in press.

Winker, C. D., ms., 1987, Neogene stratigraphy of the Fish Creek-Vallecito section, southern California: implications for early history of the northern Gulf of California and Colorado Delta: Ph.D. dissert., University of Arizona, 494 p.

Winker, C. D., and Kidwell, S. M., 1986, Paleocurrent evidence for lateral displacement of the Pliocene Colorado River delta by the San Andreas fault system, southeastern California: Geology, v. 14, p. 788–791.

Yi, Z., Ms., 1987, On the shallow hydrothermal regime of the Salton Sea geothermal field, California: M.S. thesis, University of California, Riverside, Report 87/45 of the Institute of Geophysics and Planetary Physics, 265 pp.

Zukin, J. G., Hammond, D. E., Ku, T-L, and Elders, W. A., 1987, Uranium-thorium series radionuclides in brines and reservoir rocks from two deep geothermal boreholes in the Salton Sea geothermal field, southeastern California: Geochimica et Cosmochimica Acta, v. 51, p. 2719–2732.

[AMERICAN JOURNAL OF SCIENCE, VOL. 289, JUNE, 1989, P. 708–743]

IRON-SULFUR-CARBON RELATIONSHIPS IN ORGANIC-CARBON-RICH SEQUENCES I: CRETACEOUS WESTERN INTERIOR SEAWAY

WALTER E. DEAN* and MICHAEL A. ARTHUR**

ABSTRACT. Cretaceous marine strata deposited in shallow to intermediate depths in the Western Interior seaway of North America show considerable variation in organic-carbon enrichment and degree of pyrite formation. The extreme range of paleoceanographic and depositional conditions that occurred in this seaway provide a unique opportunity to examine the effects of iron-, carbon-, and sulfur-limitation on pyrite formation in one region over about 30 my. Most of the Upper Cretaceous section consists of thick, rapidly deposited, black-shale units such as the Pierre Shale and its equivalents deposited during regressive stages of the seaway. Most of these black shales have organic-carbon contents of less than 2 percent and pyrolysis hydrogen indices that are less than 100, indicating that the organic matter is refractory. This organic matter probably was not suitable for extensive bacterial metabolism, so that pyrite formation in these shales was most likely limited by availability of reactive carbon. Two major transgressive stages of the seaway resulted in deposition of relatively thin, more slowly deposited pelagic carbonate units, the Bridge Creek Member of The Greenhorn Limestone and the Niobrara Formation. During these transgressive stages, periodic increased freshwater runoff led to increased water-column stability. These periods of increased stratification produced anoxic to slightly oxic bottom waters and enhanced preservation of primarily marine organic matter. Some of the more marly to shaly beds in each of these transgressive pelagic carbonate units have organic-carbon concentrations as high as 7 percent and pyrolysis hydrogen indices as high as 650 indicating that both units have significant hydrocarbon generating potential. All the iron in the Bridge Creek and Niobrara carbonate units apparently was reactive and has been converted to pyrite so that pyrite formation in these two units was severely iron limited. In addition, some black-shale units deposited during transgressive episodes (Mowry and Belle Fourche Shales and Sharon Springs Member of the Pierre Shale) contain abundant reactive organic matter, at least in some parts of the basin, and are iron-limited with regard to pyrite formation.

Ternary diagrams of the system Fe–S–OC, together with some measure of the reactivity of organic matter (pyrolysis hydrogen index), provide a rapid means of recognizing iron-, carbon-, and sulfur-limitation on pyrite formation in a series of samples from a single lithologic unit. Iron limitation is indicated by a concentration of data along a line of constant S/Fe ratio on a Fe–S–OC ternary diagram. Carbon limitation is indicated by a concentration of data along a line of constant S/OC ratio. Sulfur-limitation is suggested by

* U.S. Geological Survey, MS 939 Federal Center, Denver, Colorado 80225
** Graduate School of Oceanography, University of Rhode Island, Narragansett, Rhode Island 02882